Marine and Petroleum Geology 143 (2022) 105788

Contents lists available at ScienceDirect

Marine and Petroleum Geology

journal homepage: www.elsevier.com/locate/marpetgeo

Spatio-temporal variation of fluid flow behavior along a fold: The Bóixols-Sant Corneli anticline (Southern Pyrenees) from U–Pb dating and structural, petrographic and geochemical constraints

Daniel Muñoz-López [a,*], David Cruset [b], Jaume Vergés [b], Irene Cantarero [a], Antonio Benedicto [c], Xavier Mangenot [d], Richard Albert [e,f], Axel Gerdes [e,f], Aratz Beranoaguirre [e,f,g], Anna Travé [a]

[a] Departament de Mineralogia, Petrologia i Geologia Aplicada, Facultat de Ciències de la Terra, Universitat de Barcelona (UB), Martí I Franquès S/n, Barcelona, 08028, Spain
[b] Group of Dynamics of the Lithosphere (GDL), Geosciences Barcelona, GEO3BCN-CSIC, Lluís Solé i Sabarís s/n, 08028 Barcelona, Spain
[c] UMR 8148 CNRS GEOPS, Université Paris-Saclay, 91405, Orsay, France
[d] Caltech, Geological and Planetary Sciences, Pasadena, CA, USA
[e] Department of Geosciences, Goethe-University Frankfurt, 60438, Frankfurt am Main, Germany
[f] Frankfurt Isotope and Element Research Center (FIERCE), Goethe-University Frankfurt, Frankfurt am Main, Germany
[g] Departamento de Mineralogía y Petrología, Universidad Del País Vasco, Bilbao, Spain

ARTICLE INFO

Keywords:
Fluid flow
Fractures
Calcite veins
U–Pb dating
Bóixols-sant corneli anticline
Bóixols thrust sheet
Southern pyrenees

ABSTRACT

This study integrates field structural data, petrographic and geochemical ($\delta^{18}O$, $\delta^{13}C$, Δ_{47}, $^{87}Sr/^{86}Sr$, and elemental composition) analyses and U–Pb dating of calcite veins cutting the Bóixols-Sant Corneli anticline (Southern Pyrenees) in order to date and to investigate the spatio-temporal relationships between fluid flow and fold evolution. This E-W trending anticline grew from Late Cretaceous to Paleocene at the front of the Bóixols thrust sheet deforming pre-growth and growth sedimentary sequences. U–Pb dating reveals Late Cretaceous to late Miocene deformation ages, which agree with the age of growth strata deposition and the sequence of deformation interpreted from field and microstructural data. Dates coeval (71.2 ± 6.4 to 56.9 ± 1.4 Ma) and postdating (55.5 ± 1.2 to 27.4 ± 0.9 Ma) Upper Cretaceous to Paleocene growth strata are interpreted to record: (i) the growth of the Bóixols-Sant Corneli anticline during the Bóixols thrust emplacement, and (ii) the tightening of the anticline during the southern tectonic transport of the South-Central Pyrenean Unit. Other ages (20.8 ± 1.2 to 9.0 ± 4.6 Ma) postdate the folding event and have been associated with the collapse of the Bóixols-Sant Corneli anticline. The geochemistry of calcite veins indicates that the fluid flow behavior varied across the Bóixols-Sant Corneli anticline through its growth, showing a compartmentalized fluid system. In the hinge of the anticline and in the upper Santonian to middle Campanian syn-orogenic sequence along the footwall of the Bóixols thrust, the similar petrographic and geochemical features between all calcite cements and host rocks point towards a locally-derived or well-equilibrated fluid system. Contrarily, along large faults such as the Bóixols thrust, and in the anticline limbs, the geochemistry of vein cements indicates a different scenario. Cements in large faults yielded the lightest $\delta^{18}O$ values, from −8 to −14 ‰VPDB, and variable enrichment in $\delta^{13}C$, $^{87}Sr/^{86}Sr$, elemental composition and $\delta^{18}O_{fluid}$. This is interpreted as the migration of fluids, through fault zones, that evolved from distinct fluid origins. Cements in the fold limbs exhibit $\delta^{18}O$ and $\delta^{13}C$ between −8 and −6 ‰ VPDB and between −10 and + 2 ‰VPDB, respectively, the lowest Sr contents and the lowest precipitation temperatures, suggesting that the anticline limbs recorded the infiltration and evolution of meteoric waters. The paleohydrological system in the Bóixols-Sant Corneli anticline was restricted to the Bóixols thrust sheet. The Upper Triassic evaporitic basal detachment likely acted as a lower fluid barrier, preventing the input of fluids from deeper parts of the Pyrenean crustal thrust system. This study provides a well-constrained absolute timing of fracturing and fluid flow during basin inversion and folding evolution and highlights the suitability of U–Pb geochronology to refine the age of fractures and veins and their sequential evolution in orogenic belts.

* Corresponding author.
E-mail address: munoz-lopez@ub.edu (D. Muñoz-López).

https://doi.org/10.1016/j.marpetgeo.2022.105788
Received 2 February 2022; Received in revised form 7 June 2022; Accepted 9 June 2022
Available online 13 June 2022

1. Introduction

Folds are important deformation features that occur in compressional belts worldwide (Brandes and Tanner, 2014; Mitra, 1990; Vergés, 1993). Such structures have largely been a target for oil and gas exploration (Mitra, 1990), and in depleted oil fields, they depict important analogues for the assessment of CO_2 storage potential (Mitiku and Bauer, 2013). Geological storage of CO_2 (GSC) requires an appropriate reservoir placed at a suitable depth to guarantee efficiency (Alcalde et al., 2014; Bachu, 2000; Sun et al., 2020). However, the presence of fold-related fractures, which have a critical impact on the distribution of the reservoir quality, is not always easy to characterize at depth because they are usually below the resolution of standard geophysical techniques (Brandes and Tanner, 2014; Casini et al., 2011; Gutmanis et al., 2018). Therefore, the orientation, extent and the implication of such fracture systems for reservoir potential in the subsurface can only be predicted by using geological models and outcrop analogues (Brandes and Tanner, 2014; Sun et al., 2021; Tavani et al., 2015). Additionally, the formation of fold-related fractures strongly controls the origin, evolution and distribution of fluids that migrate during folding (Cosgrove, 2015; Evans and Fischer, 2012; Lefticariu et al., 2005). The appraisal of the fold-fracture relationships in natural field analogues is crucial: (i) to predict the orientation of fracture networks (fluid pathways) in areas where outcrops are absent (Bergbauer and Pollard, 2004); and, (ii) to identify the main factors controlling fluid-rock interactions in orogenic systems (Beaudoin et al., 2020; Callot et al., 2013; Ferket et al., 2006; Labeur et al., 2021; Roure et al., 2005; Swennen et al., 2000; Travé et al., 2007; Vilasi et al., 2009). Beyond this, understanding the fluid flow and deformation relationships has become of renewed interest in applied fields mainly related to climate change mitigation (Carbon Capture and Storage, CCS) and in the transition to a net zero emissions energy (exploration of natural hydrogen or geothermal anomalies, among many others) (Benedicto et al., 2021; Cooper, 2007; Macgregor, 1996; Sun et al., 2020).

Due to the economic importance of understanding the folding, fracturing and fluid flow relationships, several studies have reported the fluid system associated with the evolution of anticlines in the Pyrenees (Beaudoin et al., 2015; Cruset et al., 2016; Martinez Casas et al., 2019; Nardini et al., 2019; Sun et al., 2022; Travé et al., 2007) and in other worldwide compressional settings (Barbier et al., 2012; Beaudoin et al., 2011, 2020; Evans et al., 2012; Fischer et al., 2009; Lefticariu et al., 2005). However, these studies have mainly focused on the fracture-controlled paleohydrological evolution through time or in fluid flow associated with specific domains of the fold (Cruset et al., 2016). Thereby, the spatial variation in the fluid flow behavior and the extent of fluid-rock interaction at the different structural position of a fold have been much less documented (Evans and Fischer, 2012).

In this contribution, we report the absolute timing of deformation together with the spatio-temporal variation of the fold-fluid system and the main factors controlling the fluid origin and distribution in different structural positions of a large-scale fold, using the Bóixols-Sant Corneli anticline in the Southern Pyrenees as an example. This anticline displays excellent exposures of pre- and syn-orogenic strata involving carbonate and clastic sedimentary units (Mencos, 2010; Muñoz, 2017; Simó, 1986). This fact, together with the presence of well data and seismic reflection profiling has allowed previous studies to characterize the fold geometry and the fold-related fracture systems (Mencos, 2010; Mencos et al., 2011; Muñoz, 2017; Nardini et al., 2019; Shackleton et al., 2011; Tavani et al., 2011; Vergés, 1993). However, in this anticline, the fold-related fractures are controlled by the orientation of inherited extensional faults, resulting in asymmetric fracture networks that are neither parallel nor perpendicular to the fold axial trend (Tavani et al., 2011). Consequently, due to the asymmetrical orientation of the fractures and the absence of crosscutting relationships between most of these sets, the timing of deformation has not been entirely constrained. Hence, the main objectives of this contribution are: 1) to appraise the absolute timing of fracturing and the age and duration of fold evolution in an anticline that exhibits well-preserved growth strata that allows us to corroborate the coherence of the geochronological data; 2) to qualitatively evaluate the extent of fluid-rock interaction in fractures; 3) to decipher the origin, distribution and variation of fluids across the Bóixols-Sant Corneli anticline; and 4) to compare our results with those reported in similar compressional settings. In order to address these objectives, we provide field structural data, together with petrographic, geochemical ($\delta^{18}O$, $\delta^{13}C$, $^{87}Sr/^{86}Sr$, Δ_{47} and elemental composition) and geochronological (U–Pb ages) analyses of vein cements developed within pre- and syn-folding strata. This robust dataset has been completed with already published data from specific structures of the Bóixols-Sant Corneli anticline (Labraña de Miguel, 2004; Muñoz-López et al., 2020b; Nardini et al., 2019). Beyond the regional conclusions, our study provides a well-constrained absolute timing of deformation in an anticline that preserves pre-, syn- and post-folding fractures that do not exhibit a symmetrical orientation with respect to the fold axis, which have important implications for the interpretation of fold-fracture systems. Within this well-constrained structural setting, our study provides new constraints on the duration of fold evolution and further documents the variations and implications of the fluid flow behavior across the anticline during the entire folding event.

2. Geological setting

The Pyrenees consist of an asymmetrical and doubly verging orogenic wedge that resulted from the Alpine collision between the Iberian and European plates from Late Cretaceous to Miocene, causing the inversion of previous Mesozoic rift basins and subsequent growth of the orogenic belt (Choukroune, 1989; Grool et al., 2018; Mouthereau et al., 2014; Muñoz, 1992; Tugend et al., 2014; Vergés et al., 2002). The Pyrenean structure comprises an antiformal stack of basement-involved thrust sheets from the Axial Zone flanked by two oppositely verging fold-and-thrust belts and their related foreland basins (Fig. 1a and b) (Muñoz, 1992; Séguret and Daignières, 1986). The southern fold-and-thrust belt includes a piggy-back imbrication of Mesozoic-Cenozoic cover thrust sheets that have been detached from the Paleozoic basement along Upper Triassic evaporites (Roure et al., 1989; Séguret and Daignières, 1986). In the South-Central Pyrenees, these cover thrust sheets are, from north and older to south and younger, the Bóixols thrust sheet, active from the Late Cretaceous to Paleocene, the Montsec thrust sheet emplaced during the Paleocene to late Ypresian, and the Serres Marginals thrust sheet emplaced from Lutetian to Oligocene times (Roure et al., 1989; Vergés and Muñoz, 1990). The Bóixols thrust sheet results from the tectonic inversion of the Organyà Basin and its tectonic transport to the south. Its front corresponds to an intricate thrust fault zone of more than 40 km in length that from east to west forms the Nargó, Bóixols and Sant Corneli thrust segments, interpreted as a fault-propagation by Bond and McClay (1995), while growth anticlines formed in its hangingwall: Roca Narieda, Nargó, Bóixols and Sant Corneli (Berástegui et al., 1990). This study focuses on the westernmost section of these growth folds that corresponds to the Bóixols-Sant Corneli anticline (Fig. 2a and b).

The complete stratigraphic record involved in the Bóixols-Sant Corneli anticline includes Upper Triassic to Upper Cretaceous pre-orogenic rocks and Upper Cretaceous to Paleocene syn-orogenic units (Berástegui et al., 1990; Mencos et al., 2015; Simó, 1986) (Fig. 2c). The pre-orogenic sequence includes up to 5 km of pre-rift, syn-rift and post-rift (pre--orogenic) rocks located in the hanging wall of the Bóixols thrust. The pre-rift sequence, which is up to a few thousand meters thick (Lanaja, 1987; Mencos et al., 2011), crops out discontinuously in the study area and includes Upper Triassic shales and evaporites, which constitutes the main detachment level in the Pyrenees, and Jurassic dolomitic limestones and dolostones. The Lower Cretaceous syn-rift sequence extensively crops out in the hinge of the anticline. This sequence ranges from a few meters to more than 4000 m thick, and includes an intercalation of

basinal marls, marly limestones and limestones (i.e., the Lluçà Formation), which lower part abruptly evolves to platform limestones (the Setcomelles Member) (Berástegui et al., 1990; García-Senz, 2002).

The upper Cenomanian to lower Santonian post-rift (pre-orogenic) sequence is around 800 m thick and mainly consists of carbonate rocks divided in five sedimentary formations, which in the study area are known as the Santa Fe, the Reguard, the Congost, the Collada Gassó and the Sant Corneli Formations (Gallemí Paulet et al., 1982; Mencos, 2010; Simó, 1986).

The syn-orogenic sequence is well-exposed in the footwall of the

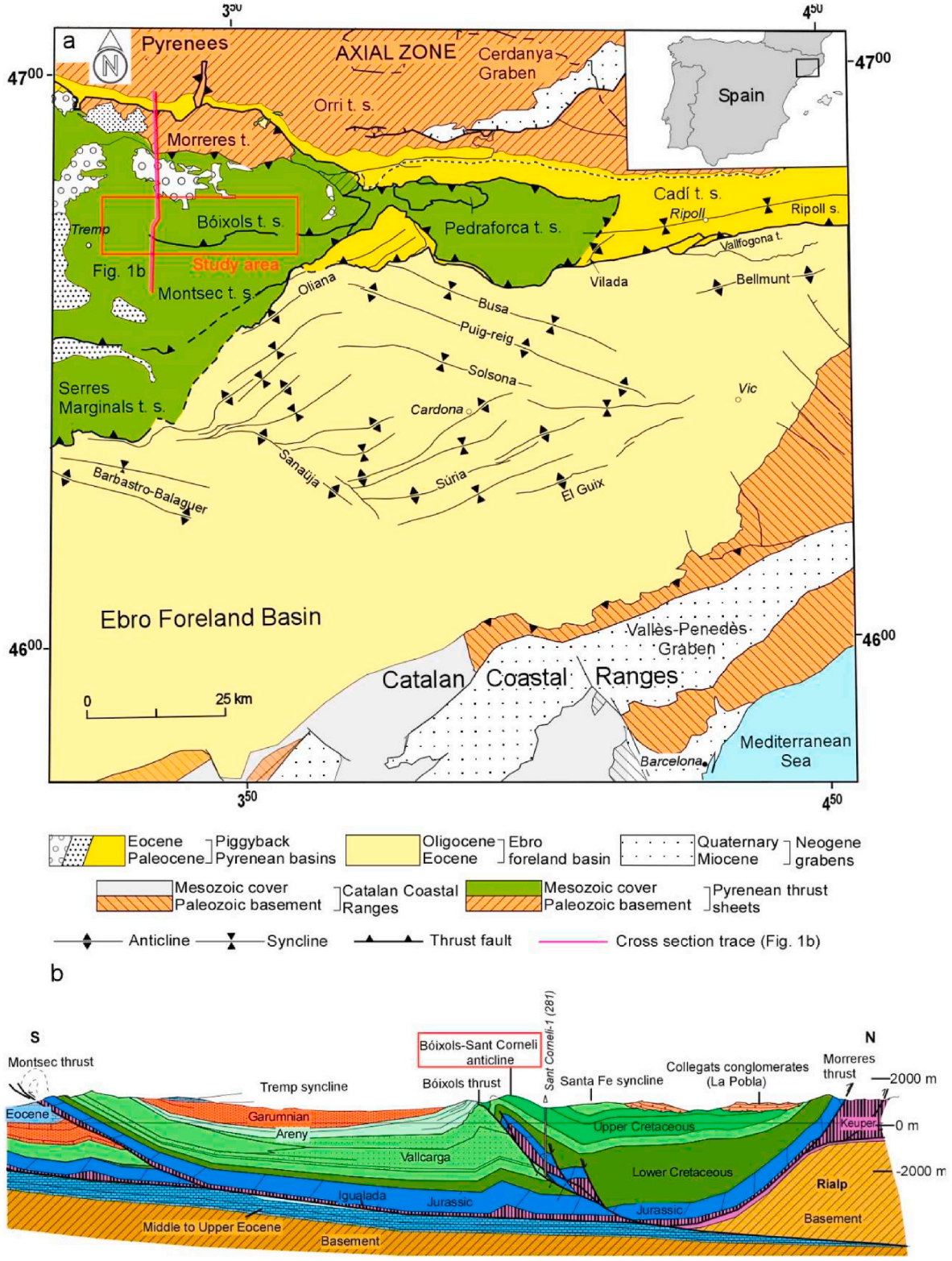

Fig. 1. (a) Simplified geological map and (b) cross-section of the main structural units from the south Pyrenean fold-and-thrust belt (Vergés, 1993). The red square indicates the location of the Bóixols-Sant Corneli anticline along the front of the Bóixols thrust sheet. (For interpretation of the references to color in this figure legend, the reader is referred to the Web version of this article.)

Bóixols thrust and includes more than 1000 m of upper Santonian to Paleocene sedimentary rocks exhibiting growth geometries. These syn-orogenic rocks, which have been dated using biostratigraphy (Gómez-Garrido, 1987; Mencos, 2010; Mercedez, 2005; Simó, 1986), comprise three shallowing upward sequences grading from turbidites and marls into shallow marine, fluvial and continental deposits (Mencos, 2010; Mey et al., 1968). These three sequences belong to the Vallcarga Formation and to the Areny and the Tremp Groups. The Vallcarga Formation (upper Santonian to middle Campanian) mainly consists of hemipelagic marls. The middle part of this formation consists of a slope-toe chaotic unit (i.e., the Puimanyons Member) developed due to the destabilization of the carbonate platform and characterized by growth faulting and olistostrome resulting from basin margin collapse during the growth of the Bóixols-Sant Corneli (Bond and McClay, 1995; Simó, 1986). The Areny Group (late Campanian to Maastrichtian) deposited during the Bóixols thrust activity and related Bóixols-Sant Corneli anticline growth (Bond and McClay, 1995; Mencos et al., 2011; Robert et al., 2018). This sequence mainly consists of shallow marine to coastal deposits. Finally, the Maastrichtian to Paleocene Tremp Group (i.e., Garumnian facies) includes alluvial, fluvial, lacustrine and carbonate deposits.

The structure of the Bóixols thrust sheet is composite, formed by the large Santa Fe syncline and the two linked and south-verging anticlines of Bóixols and Sant Corneli (the Bóixols-Sant Corneli anticline) (Fig. 2a and b). The surficial expression of the Bóixols-Sant Corneli anticline crops out along more than 40 km showing a well-defined geometry in its central-western segment that is characterized by a gently dipping (around 40°) northern backlimb and a subvertical to overturned southern forelimb.

During the inversion of the Bóixols thrust and growth of the Bóixols-Sant Corneli anticline along its front, shortening direction has been determined as NNW-SSE (Tavani et al., 2011). This orientation, which is not perpendicular but slightly oblique to E-W trending inverted normal fault, strongly conditioned the orientation of fractures developed during the evolution of this frontal anticline (Shackleton et al., 2011; Tavani et al., 2011).

The Bóixols thrust along the forelimb of the Bóixols-Sant Corneli anticline is well preserved, near the villages of Bóixols and Abella de la Conca (Fig. 2). Contrarily, around the Coll de Nargó locality, the Bóixols thrust is blind and sealed by syn-orogenic deposits and the southern limb of the Bóixols anticline is cut by decametric to kilometric subvertical strike-slip faults (e.g., Nardini et al., 2019) (Fig. 2). The northern limb of the Bóixols-Sant Corneli anticline is cut by well-preserved large normal faults displacing Upper Cretaceous carbonate sequences in Montagut and Sant Joan localities. All these fractures record a significant part of the structural and fluid flow histories of the Bóixols thrust sheet, which preserves both pre- and syn-orogenic deformation.

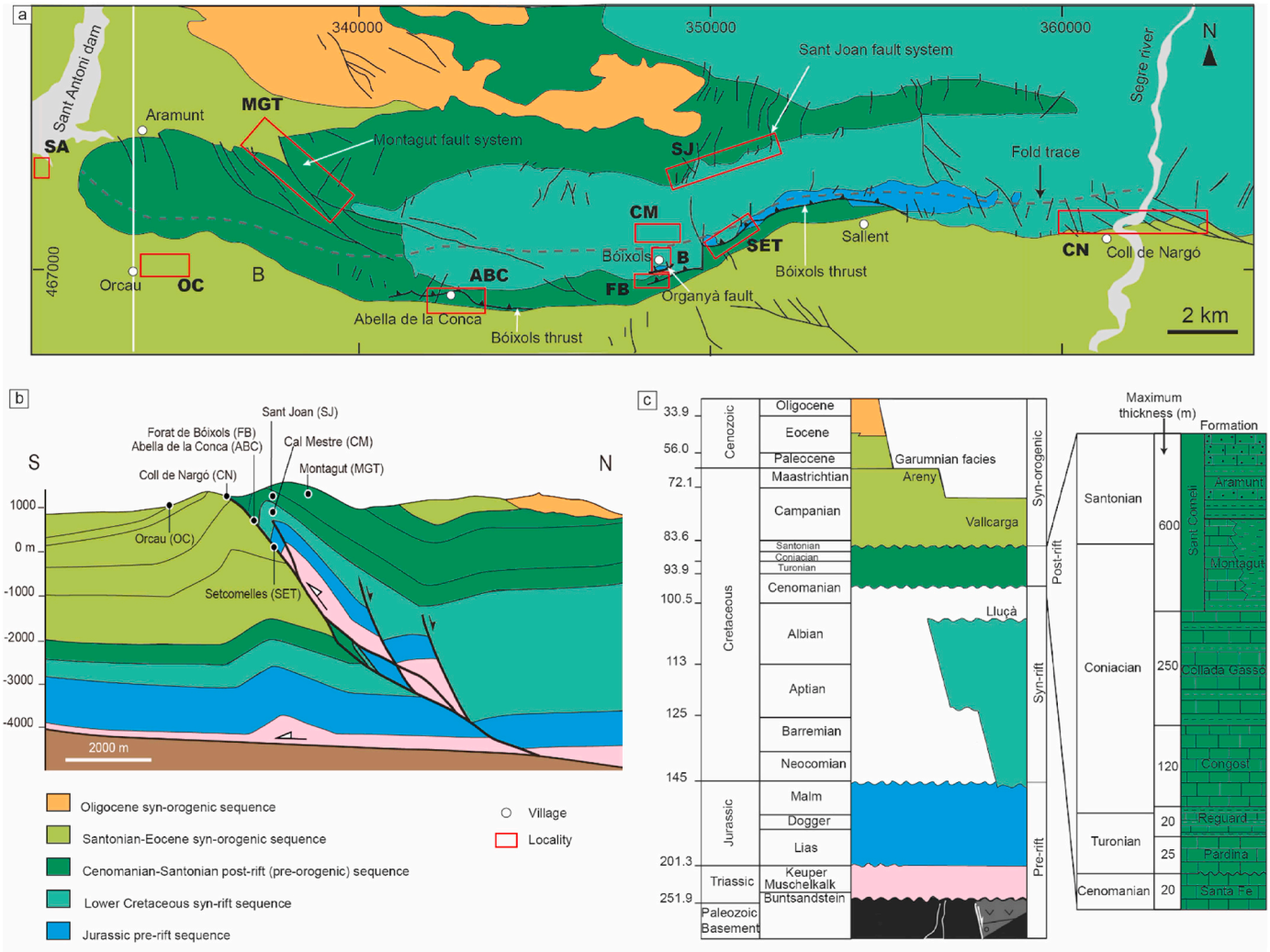

Fig. 2. (a) Simplified geological map (Mencos, 2010; Tavani et al., 2011) and (b) cross-section (Vergés, 1993) of the Bóixols-Sant Corneli anticline showing the studied localities. (c) Chronostratigraphic diagram displaying the main stratigraphic sequences found around the Bóixols-Sant Corneli anticline and their associated tectonic event (Mencos et al., 2015). Location of map and cross-section in Fig. 1a.

3. Methodology

This study integrates field, petrographic, geochemical, and geochronological analyses of vein cements and related host rocks from 10 representative localities (Figs. 3 and 4). The field data comprise bedding and fracture dips and dip directions and their crosscutting relationships and kinematics. Such data are plotted in equal-area lower-hemisphere stereoplots to define different fracture systems. Restoration of these fracture systems with respect to the adjacent bedding and estimation of the associated stress orientations have been carried out using Win-Tensor software (Delvaux and Sperner, 2003). For analysis of fault kinematics, this software considers the improved Right Dihedron method (Angelier, 1984), which is an inversion technique that under basic assumptions and limitations (Lacombe, 2012), allowed us to calculate paleostress orientations and stress ratios for the different striated faults present in the study area.

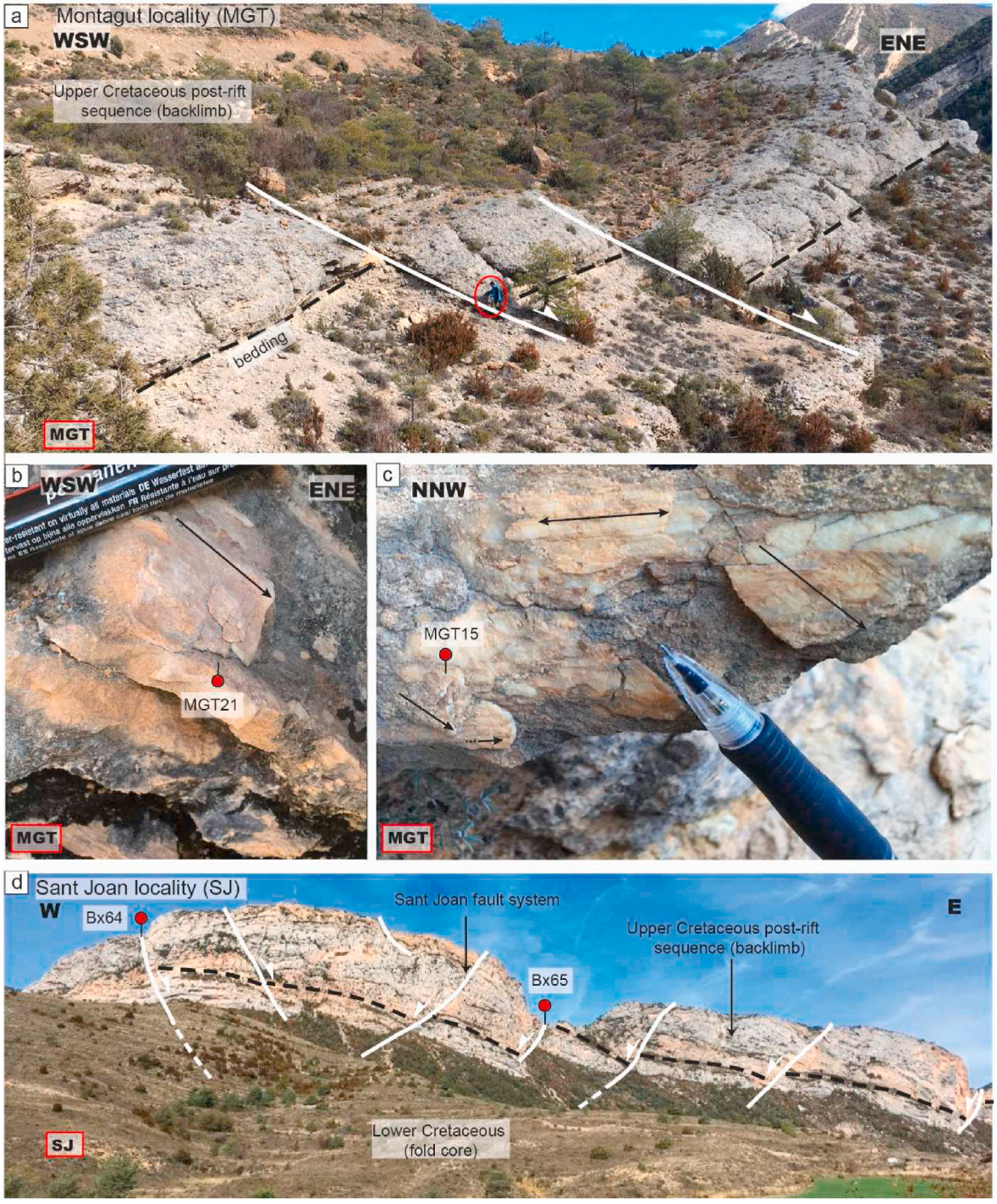

Fig. 3. Field images showing the main features of Montagut and Sant Joan localities. (a) and (b) Montagut locality showing NNW-SSE tilted extensional faults affecting the Upper Cretaceous sequence in the backlimb of the Bóixols-Sant Corneli anticline. (c) In the same Montagut locality, some fault surfaces exhibit crosscutting relationships between striae sets that indicate either oblique-slip or strike-slip kinematics. (d) Sant Joan locality showing the main NNE-SSW extensional faults also affecting the Upper Cretaceous sequence in the backlimb. Red circles indicate sample location. (For interpretation of the references to color in this figure legend, the reader is referred to the Web version of this article.)

Fig. 4. Field images showing the main features of Abella de la Conca, Forat de Bóixols, Setcomelles and Sant Antoni localities. (a) and (b) the Bóixols thrust in the Abella de la Conca and Forat de Bóixols localities, respectively, offsetting the steeply dipping Upper Cretaceous sequence located in the forelimb of the Bóixols-Sant Corneli anticline. (c) The main Bóixols thrust in the Setcomelles locality juxtaposing Jurassic dolomitized limestones in its hanging wall with Upper Cretaceous limestones in its footwall. (d) Fault surface showing crosscutting relationships of superimposed striae sets, where a normal displacement is postdated by a later strike-slip movement. This fault affects the base of the syn-orogenic sequence located in the footwall of the Bóixols thrust sheet. Red circles indicate sample location. (For interpretation of the references to color in this figure legend, the reader is referred to the Web version of this article.)

Up to 185 samples of the involved host rocks and all vein cement generations filling the recognized fractures systems have been selected for petrographic, geochemical and geochronological analyses. Around 135 polished thin sections of these samples have been analyzed for petrographic descriptions with a Zeiss Axiophot microscope and a cold cathodoluminescence (CL) microscope operating at 15–18 kV and 350 μA current.

Geochemical analyses have been applied to vein cements and host rocks in order to determine the origin, distribution and temperature of the vein-forming fluids as well as the extent of fluid-rock interaction. These geochemical data consist of (i) stable isotope analysis of 150 representative samples, (ii) the elemental composition of 69 samples, (iii) the $^{87}Sr/^{86}Sr$ ratios of 43 samples, (iii) clumped isotope thermometry of 21 samples, the results of which were converted to temperatures by applying the calibration method of (Kluge et al., 2015). Calculated $\delta^{18}O_{fluid}$ values are expressed in per mill (‰) with respect to the Vienna Standard Mean Ocean Water (VSMOW). This study also includes U–Pb dates obtained with a laser ablation-inductively coupled plasma mass spectrometer (LA-ICPMS) at FIERCE (Frankfurt Isotope and Element Research Center, Goethe University). Details on the different methods and procedures can be found in the supplementary material.

4. Results

4.1. Studied localities

The studied localities record the deformation history and fluid flow events that occurred in the Bóixols-Sant Corneli anticline (Figs. 3 and 4). Therefore, ten sampling localities were selected as representative of the different fracture networks as well as the involved host rocks already described in the geological setting. The main characteristics of these localities are described below.

The Bóixols locality (B) is located in the Bóixols village, next to the axial surface of the anticline. In this locality, the contact between the Lower Cretaceous limestones and marls from the syn-rift sequence and the Jurassic dolomitic limestones from the pre-rift succession has been interpreted as the preserved upper part of the main E-W Early Cretaceous extensional fault (e.g., Berástegui et al., 1990; Tavani et al., 2011).

The Cal Mestre locality (CM) is located 0.5 km to the northeast of the Bóixols village, in the hinge of the Bóixols anticline. In this area, the Lower Cretaceous limestones and marls from the syn-rift sequence are broadly exposed exhibiting a minimum thickness of 2500 m according to well data (Lanaja, 1987).

The Montagut (MGT) and the Sant Joan (SJ) localities are in the northern limb of the anticline, affecting Upper Cretaceous limestones from the post-rift (pre-orogenic) sequence. The structure of the Montagut locality consists of relatively well exposed systems of normal, oblique-slip and strike-slip faults with a lateral continuity of several kilometers (Fig. 3a–c) (i.e., the Montagut fault system). The structure of the Sant Joan locality includes two conjugate sets of strike-slip faults and a different set of normal faults. The latest set is referred in this study as the Sant Joan fault system (Fig. 3c).

The remaining localities are located along the frontal region of the Bóixols thrust sheet and include fractures that cut pre-orogenic depositional units from the southern limb of the Bóixols-Sant Corneli anticline and syn-orogenic units deposited in the footwall of the Bóixols thrust sheet. The Bóixols thrust has been studied in Abella de la Conca (ABC), Forat de Bóixols (FB) and Setcomelles (SET) localities (Fig. 4a–c). In Abella de la Conca and Forat de Bóixols localities, the E-W trending and north-dipping Bóixols thrust offsets subvertical post-rift Upper Cretaceous limestones along the southern limb of the Bóixols-Sant Corneli anticline. The Abella de la Conca locality also includes a reduced Upper Cretaceous syn-orogenic sequence. The Forat de Bóixols locality, located 2 km southwest of the Bóixols village, preserves a good exposure that allowed to study the evolution of fractures across the Bóixols thrust zone in a previous paper (Muñoz-López et al., 2020b) (Fig. 4b). In the Setcomelles locality, between Bóixols and Sallent villages, the Bóixols thrust is interpreted as a footwall shortcut of the previous Lower Cretaceous Organyà fault. In this area, Jurassic dolomitized limestones juxtapose against Upper Cretaceous limestones (García-Senz, 2002) (Fig. 4c). The Sant Antoni (SA), Orcau (OC) and Coll de Nargó (CN) localities are aligned along the footwall of the Bóixols thrust, involving Upper Cretaceous to Paleocene syn-orogenic sequences showing growth strata patterns (Bond and McClay, 1995; Garrido-Megías et al., 1972; Mencos et al., 2011; Tavani et al., 2017; Vergés and Muñoz, 1990). The Sant Antoni locality, next to the Sant Antoni dam, comprises the lowest part of the syn-orogenic sequence integrated in the Vallcarga Fm. (Fig. 4d). The Orcau locality, next to the Orcau village, constitutes the middle part of the syn-orogenic unit integrated in the Areny Group. Finally, the Coll de Nargó locality, near the Coll the Nargó village, involves the upper part of the syn-orogenic sequence integrated within the Garumnian facies from the Tremp Group. In this area, the Bóixols thrust is buried and the syn-orogenic deposits are deposited in angular unconformity on the front of the anticline and are affected by conjugated systems of veins and strike-slip faults (i.e., the Coll de Nargó faults) (Nardini et al., 2019).

4.2. Petrographic description of host rocks

In this section, we summarize the main petrographic features of the studied host rocks. The syn-rift Lower Cretaceous Lluçà Formation, made up of mudstones with isolated sponge spicules and agglutinated foraminifera (Fig. 5a), features a dark brown to non-luminescence (Fig. 5b). The lower part of the Lluçà Fm (the Setcomelles Member) is formed of wackestones, locally packstones, made up of corals, red algae (*Agardhiellopsis cretacea*), echinoderms, bryozoans and foraminifera. The moldic porosity is filled with micrite sediment with a geopetal distribution, which indicates vadose environment, and the remanent intraparticle porosity is filled by calcite cement (Fig. 5c). The micrite matrix exhibits a brown to dark orange luminescence, whereas the intraparticle micrite sediment shows an orange luminescence and the cement has a non-to bright yellow zonation (Fig. 5d).

The Upper Cretaceous post-rift (pre-orogenic) sequence includes five sedimentary formations, which are known as the Santa Fe, the Reguard, the Congost, the Collada Gassó and the Sant Corneli Formations. The Santa Fe Fm., including wackestones, locally packstones with calcispheres and planktonic foraminifera, exhibits a very dark orange luminescence. The Reguard Fm. consists of mudstones, locally wackestones, made up of foraminifera (mainly miliolids) and showing a dark brown luminescence. The Congost Fm. is made up of packstones, locally grainstones formed of bivalves, foraminifera, echinoderms, corals, bryozoans and partially to totally micritized components (i.e., peloids) (Fig. 5e). The micritic matrix and the inter- and intraparticle blocky calcite cement are dark brown to non-luminescent (Fig. 5f). The Collada Gassó Fm. is formed of grainstones made up of gastropods, bivalves, echinoids, corals, bryozoans, miliolids, peloids, and locally quartz grains. The inter- and intraparticle porosity is cemented by blocky calcite cement, which exhibits a bright yellow luminescence, whereas the skeletal components display a dull to bright brown luminescence. The Sant Corneli Fm. is divided in two members (the Montagut Mb and the Aramunt Vell Mb). The Montagut Mb. consists of peloidal wackestones to packstones with abundant presence of rudists, miliolids, corals, equinoderms and local quartz detrital components. Under cathodoluminescence, these packstones exhibit a dark to bright brown color. The Aramunt Vell Mb. consists of bioclatic grainstones with variable quartz content and abundant presence of miliolids, bryozoans, equinoderms and bivalves. The interparticle calcite cement is blocky and displays a dark orange luminescence.

The Upper Cretaceous to Paleocene syn-orogenic successions include the Vallcarga Formation, the Areny Group and the Tremp Group (Garumnian facies). The Vallcarga Formation consist of mudstones that are brown to non-luminescent (Fig. 5g–h). The Areny Group, in the study

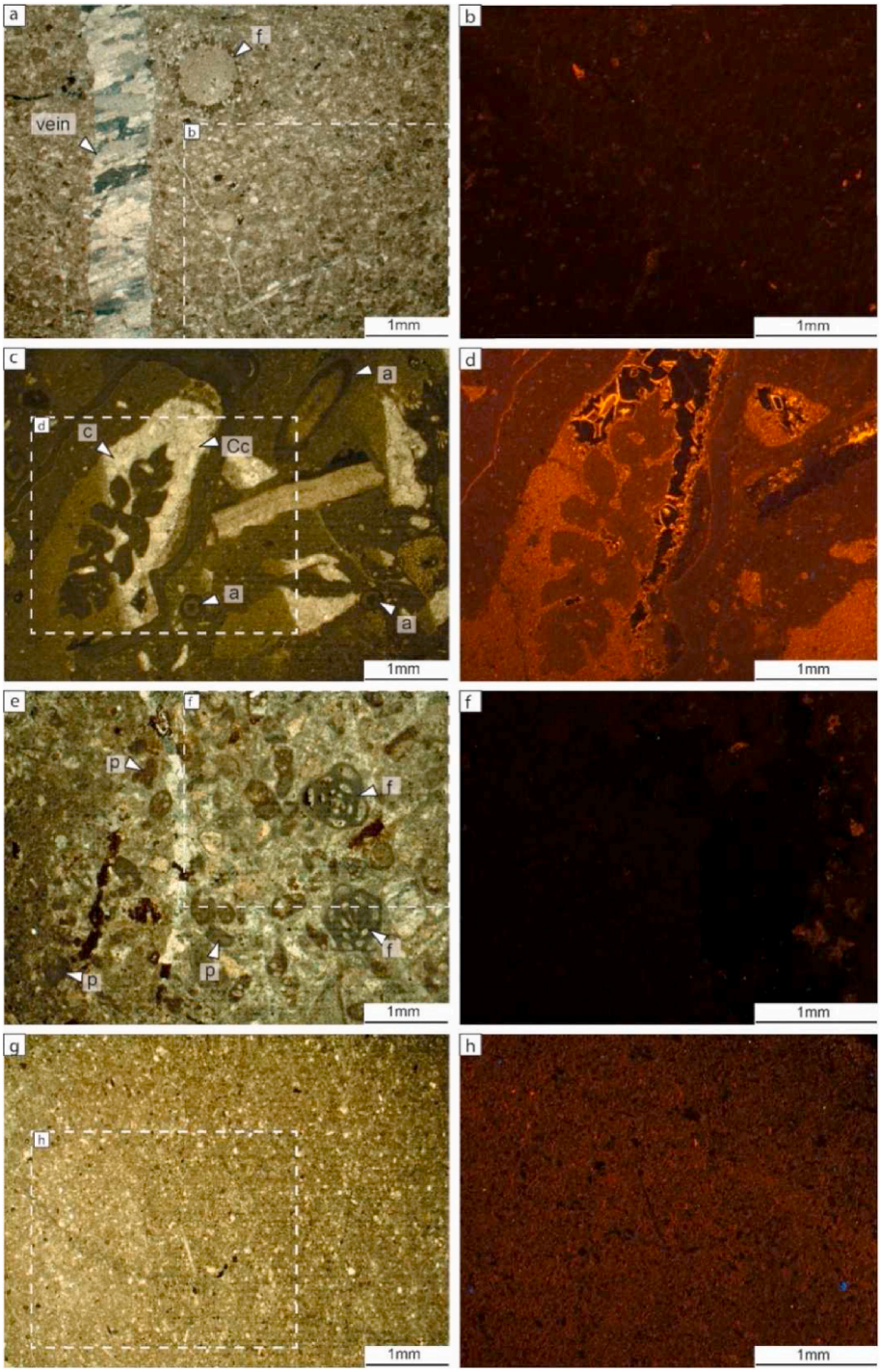

Fig. 5. Paired optical and CL microphotographs showing the main petrographic characteristics of the studied host rocks. (a) and (b) Mudstones from the Lower Cretaceous Lluçà Fm. with an isolated agglutinated foraminifera [f] and featuring a dark brown luminescence. (c) and (d) Wackestones to packstones from the Lower Cretaceous Setcomelles Mb made up of corals [c], red algae [a], presence of micritic sediment filling moldic porosity with a geopetal distribution and calcite cement [Cc] filling the rest of the intraparticle porosity. The micritic matrix has a brown to dark orange luminescence, the intraparticle micrite sediment has an orange luminescent and the intraparticle cement is zonated, varying from a non-luminescence to bright yellow. (e) and (f). Packstones to grainstones from the Upper Cretaceous Congost Fm. with abundant presence of foraminifera [f] and peloids [p] and displaying a non-luminescence. (g) and (h) Mudstones from the Vallcarga Fm. featuring a brown luminescence. (For interpretation of the references to color in this figure legend, the reader is referred to the Web version of this article.)

localities, is composed of grainstones made up of peloids, local bryozoans and miliolids, and upward increasing detrital quartz content. The interparticle blocky calcite cement is bright yellow luminescent. The Tremp Group (i.e., Garumnian facies) is constituted of fluvial-alluvial and lacustrine detrital and carbonate rocks. Detrital units include versicolored clays with abundant Microcodium, fine-grained sandstones and polymictic conglomerates. Carbonate units include red nodular mudstones, grey wackestones with charophytes and oncolytic packstones.

4.3. Fracture analysis

The folded sequence within the Bóixols-Sant Corneli anticline is affected by several fracture sets that include the main reverse, strike slip and normal faults affecting the anticline (the Bóixols thrust, the Montagut fault system and the Sant Joan fault system) and the background deformation (centimetric to metric fractures). We use the term "fracture" or "joint" to include fractures that show no evidence of shear, and we use the term "fault" to exclusively include shear fractures (Bons et al., 2012). The main fracture and fault characteristics (type, orientation, kinematics, and crosscutting relationships) and their distribution within the anticline are described below.

Thrust faults are important deformation features affecting the frontal part of the Bóixols-Sant Corneli anticline (in the Setcomelles, Forat de Bóixols and Abella de la Conca localities). Thrusts are E-W trending and south verging reverse faults dipping between 15° to 30° towards the north. These faults include the main Bóixols thrust that has been associated with the growth of the Bóixols-Sant Corneli anticline. Although most of the Bóixols fault trace has been buried by syn-orogenic deposits, its frontal ramp crops out between Bóixols and Sallent villages (Setcomelles locality) juxtaposing Jurassic rocks of the hanging wall with Upper Cretaceous carbonates of the footwall. In this locality, the Bóixols thrust zone is around 15-m-thick and contains a 2-m-thick fault core characterized by a dark grey to greenish fine-grained foliated gouge featuring well-developed S–C structures that indicate top-to-the S and SSE reverse kinematics.

In the Forat the Bóixols and in Abella de la Conca localities, the Bóixols thrust displaces, and postdate, the vertical to overturned southern forelimb of the Bóixols-Sant Corneli anticline generating well-exposed fault zones. These fault zones consist of up to 7 m thick light grey and fine-grained foliated gouges characterized by well-developed S–C structures forming sigmoidal lenses or imbricated lithons, which are bounded by pressure-solution seams or stylolites striking WSW-ENE. The orientation of these stylolites suggests an NNW-SSE shortening direction, and the presence of striation surfaces on the main slip planes together with the S–C structures also indicate reverse kinematics towards the S-SE. The damage zones, surrounding these fault cores, are characterized by different sets of systematically and randomly-oriented calcite veins exhibiting an increase in vein density from the protolith towards the fault core, as described in Muñoz-López et al. (2020b).

Additionally, strike slip faults are also important deformation features that have been observed in most of the studied localities affecting the different structural and stratigraphic positions of the Bóixols-Sant Corneli anticline. In the Montagut and Cal Mestre localities, WNW-ESE right-lateral strike slip faults cut pre-orogenic units. These faults developed during the strike-slip reactivation of earlier extensional faults due to their favorable orientation with respect to N–S to NNW-SSE shortening direction as evidenced by the presence of slickenlines and striae sets showing crosscutting relationships (Martinez Martinez Casas et al., 2019; Nardini et al., 2019; Tavani et al., 2011). In other localities, N–S to NW-SE and less abundant NE-SW strike slip faults are mainly subvertical, regardless of the bedding dips, and show displacements from a few centimeters up to several meters. Deformation associated with these faults is either localized on discrete polished slip surfaces or accommodated along an up to 1-m-thick fault cores formed of brittle incohesive fault rocks. Sub-horizontal slickenlines present on the slip planes indicate pure strike-slip, and locally oblique-slip, kinematics. These faults affect pre-orogenic units in the backlimb (Montagut and Sant Joan localities) and the hinge (Cal Mestre locality) of the Bóixols-Sant Corneli anticline and syn-orogenic units (Sant Antoni and Coll de Nargó localities).

Normal faults widely occur in the Bóixols-Sant Corneli anticline. In the pre- and syn-rift sequence (Bóixols and Cal Mestre localities), normal faults strike WNW-ESE to NW-SE and dip 40° to 70° towards the NE and SW. These faults include the Organyà fault, preserved next to the axial surface of the anticline juxtaposing Jurassic pre-rift and Lower Cretaceous syn-rift sequences, and meter-scale normal faults that only affect the Lower Cretaceous (syn-rift) Lluçà Formation. In the backlimb of the Bóixols-Sant Corneli anticline, normal faults have been observed around the Montagut and the Sant Joan fault systems (Montagut and Sant Joan localities, respectively) cutting the Upper Cretaceous pre-orogenic sequence. In the Montagut locality, metric to decametric NNW-SSE extensional faults dip 50° to 80° either towards the SW or NE. Deformation associated with these faults is mainly localized in discrete slip planes exhibiting subvertical striae sets or in centimetric fault cores constituted of grey to reddish calcite-cemented breccias. In the San Joan locality, metric to decametric NNE-SSW to NE-SW extensional faults dip around 60° towards the NW and SE. These faults present subvertical striae sets indicating dip-slip kinematics and have also been observed in the Santa Fe syncline (i.e., in the north of the Bóixols-Sant Corneli anticline). Finally, WNW-ESE extensional faults dipping between 40° and 80° towards the NE and SW have been locally observed in the syn-orogenic succession in the Sant Antoni locality and locally in the syn-orogenic sequence from the Abella de la Conca locality.

Bed-parallel slip surfaces are commonly developed between well-bedded layers of marls and marly limestones in the syn-rift sequence (Cal Mestre locality) and the base of the syn-orogenic sequence (Sant Antoni and Abella de la Conca localities) of the Bóixols-Sant Corneli anticline. These surfaces correspond to centimeter-thick and striated discrete planes cemented by calcite.

Other mesostructures occurring in most structural positions of the Bóixols-Sant Corneli anticline correspond to calcite-cemented fractures (i.e., veins) oriented at high angle with respect to bedding. NNW-SSE and NNE-SSW centimetric vein systems dipping between 50° and 80° have been observed in the backlimb and forelimb of the anticline (Sant Joan and Coll de Nargó localities, respectively) affecting pre-orogenic units. These veins have regular shapes and show openings ranging from 1 to 15 mm. E-W to WSW- ENE calcite veins are also present in the pre-orogenic unit (Cal Mestre locality) and in the syn-orogenic sequence (Orcau and Abella de la Conca localities). These veins are up to 1 m long and less than 1 cm thick. In the Orcau locality, veins with similar NW-SE orientation show crosscutting relationships suggesting development of similar fractures during successive fracturing events.

4.4. Petrographic description of vein cements

The petrographic description of the different vein cements from fractures using optical and cathodoluminescence (CL) microscopes is summarized in this section and in Fig. 6.

Calcite cements precipitated within faults and related fractures across the Bóixols-San Corneli anticline are characterized by elongated to fibrous crystals ranging in size from 0.1 to 7 mm, although most common crystals are less than 2 mm (Fig. 6a). Luminescence features of these cements are generally very homogeneous and vary from dark brown to bright yellow, being dull orange to dark yellow the most common colors observed under CL (Fig. 6b).

Cements from veins that precipitated in bed-parallel slip surfaces share similar petrographic characteristics throughout the Bóixols-Sant Corneli anticline. These cements, which consist of up to 5 mm elongated to fibrous calcite crystals arranged parallel to both the vein walls and the bedding surfaces, are dark brown to non-luminescent (Fig. 6c–d).

Calcite cements precipitated in centimetric to metric non shear fractures are mainly characterized by blocky to elongated blocky crystals ranging in size from 0.2 to 5 mm and locally displaying mechanical twining (Fig. 6e–f). Elongated blocky calcites have been observed in different veins exhibiting elongation direction perpendicular to fracture walls and indicating the mode I opening of the vein (Bons et al., 2012) (Fig. 6f). Under CL, cements within non-shear fractures display three kind of luminescence colors: (i) dark brown to non-luminescence; (ii) orange to bright yellow; and (iii) a non-luminescent to bright yellow concentric zonation (Fig. 6g–h).

Besides, it is worth noting two correlations observed between the luminescence features of the vein cements and the structural position of the Bóixols-Sant Corneli fold. First, all cements from fractures present in two localities (Cal Mestre and Sant Antoni localities, which are found in the fold hinge and in the base of the syn-orogenic deposits along the footwall of the Bóixols thrust, respectively) exhibit a dark brown to non-luminescence. This is the case, for instance, of the veins from bed-parallel slip surfaces explained above (Fig. 6c–d). Second, all cements showing a non-luminescent to bright yellow concentric zonation are found in fractures present in the limbs of the anticline, this is, in Sant Joan and Forat de Bóixols localities as shown in Fig. 6g–h.

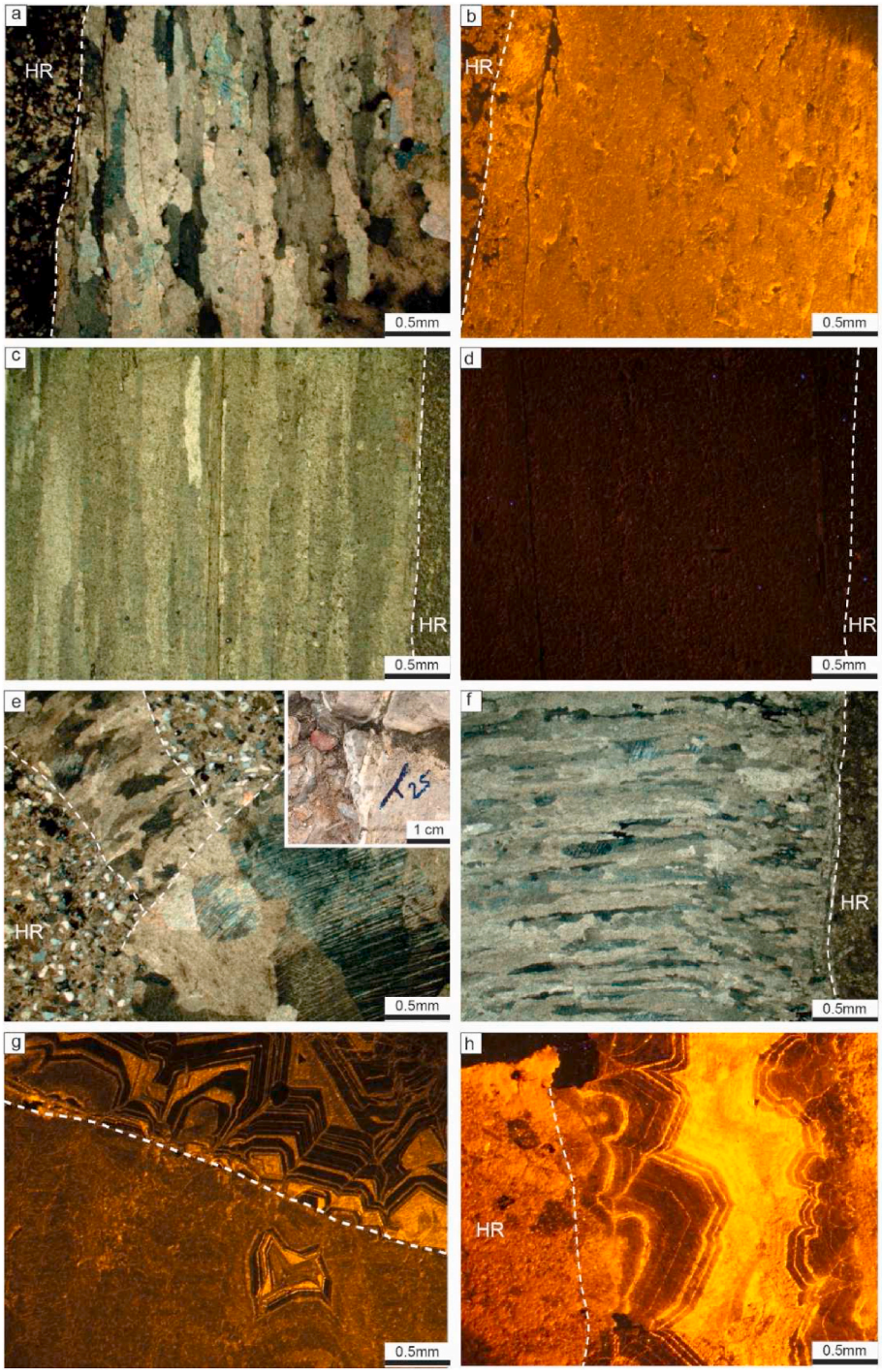

Fig. 6. Optical and CL microphotographs showing the main textural features of the studied calcite cements. (a) and (b) cement from a strike slip fault with an elongated blocky texture and a dull yellow luminescence. (c) and (d) cement from a bed-parallel slip surface with an elongated to fibrous texture and a dark to non-luminescence. (e) Crosscutting relationships between vein cements where a blocky calcite crosscut an elongated blocky cement. (f) Elongated cement where calcite crystals grow perpendicularly to the fracture walls indicating the opening mode of the vein. (g) Cement with a non-luminescent to bright yellow zonation postdating another cement that displays a dark yellow luminescence. (h) Cement from a vein showing a blocky texture and exhibiting a concentric zoned luminescence. (For interpretation of the references to color in this figure legend, the reader is referred to the Web version of this article.)

4.5. Geochemistry of calcite cements and host rocks

Stable ($\delta^{18}O$ and $\delta^{13}C$) and clumped (Δ_{47}) isotopes, $^{87}Sr/^{86}Sr$ ratios and elemental composition of the successive calcite veins and related host rocks are summarized in Figs. 7–9 and in the supplementary data. In order to discuss all the complexity of the geochemical values, the studied calcite cements have been assembled in three groups (Figs. 7–9), according to similarities of the main geochemical features:

Group 1 includes dark to non-luminescent calcite cements, similar to their adjacent marine host rocks, either the Lower Cretaceous marls of the Lluçà Formation or the Upper Cretaceous marls of the Vallcarga Formation. These cements also show $\delta^{13}C$ values and $^{87}Sr/^{86}Sr$ ratios similar to their adjacent host rocks, which are typical of marine carbonates (Figs. 7 and 8) (Veizer et al., 1999). They are also characterized by Sr contents higher than 1100 ppm, Mn contents lower than 200 ppm, and Y/Ho ratios higher than 50 (Fig. 9). The $\delta^{18}O$ values of Group 1 cements are similar to or up to 5 ‰VPDB lighter than those values of their correspondent host rocks (Figs. 7 and 8b). Their geochemistry generally reflects the composition of their host carbonates. Cements from Group 1 are all cements from fractures and faults present in the hinge of the anticline (Cal Mestre locality) and in the base of the syn-orogenic deposits in the footwall of the Bóixols thrust sheet (Sant Antoni locality). In addition, 9 representative samples of this Group were analyzed to reconstruct the temperature and composition of the

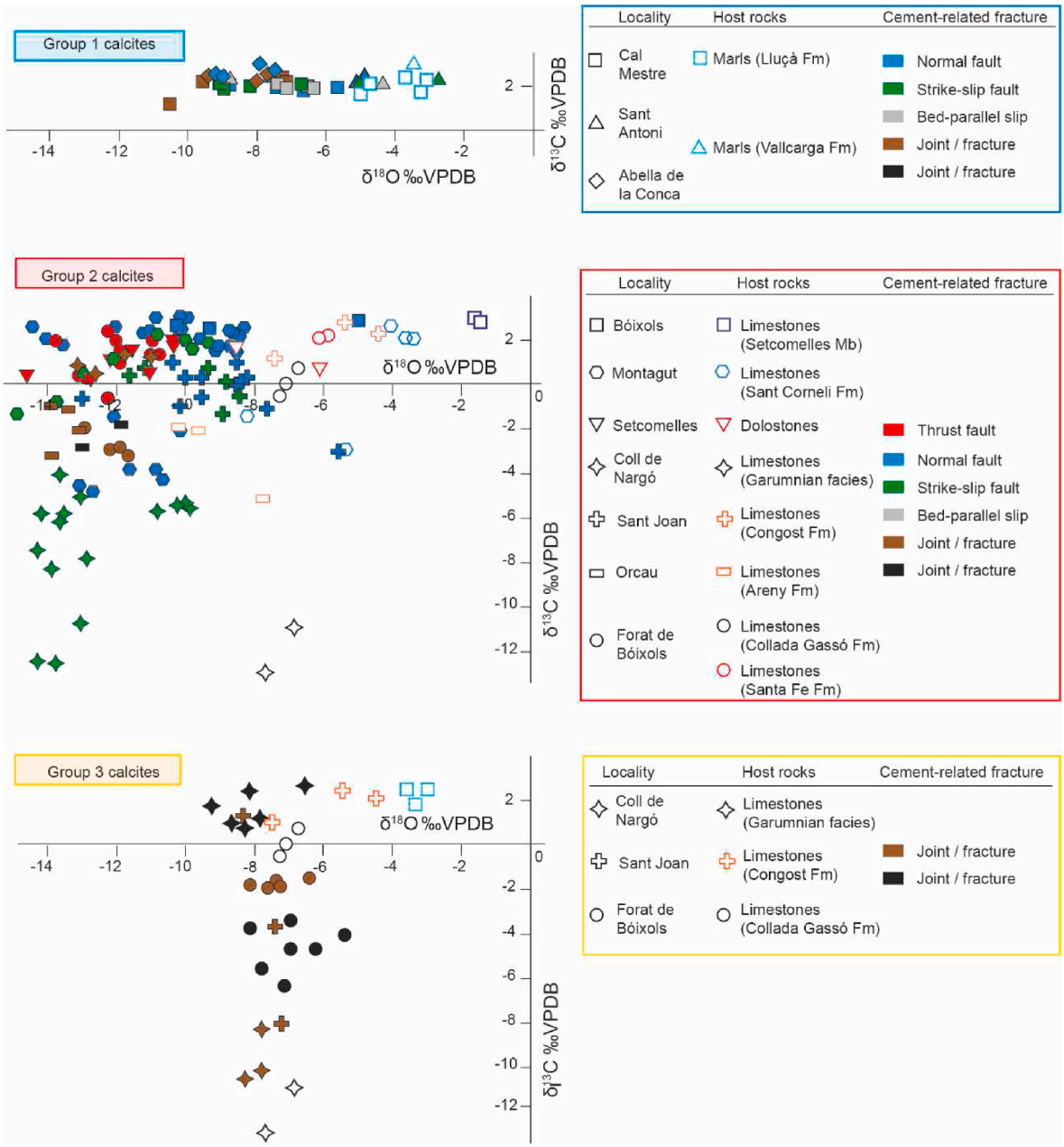

Fig. 7. Stable isotopic composition ($\delta^{18}O$ vs $\delta^{13}C$) of the three groups of calcite cements and related host rocks. Solid symbols refer to calcite cements from fractures and open symbols refer to their associated host rocks (the different symbols represent localities where samples were taken).

fluids precipitating these cements using clumped isotope measurements. In the hinge of the anticline (5 samples), the obtained Δ_{47} values range from 0.456 to 0.567 ± 0.028, which translates into precipitation temperatures ranging from 36 to 85 °C and $\delta^{18}O_{fluid}$ varying from −4.7 to +3.8 ‰SMOW. In the base of the syn-orogenic deposits from the footwall of the Bóixols thrust sheet (4 samples) the Δ_{47} values vary from 0.404 ± 0.022 to 0.509 ± 0.015, which indicates precipitation temperatures ranging from 59 to 116 °C and $\delta^{18}O_{fluid}$ from +5.3 to +6.5 ‰ SMOW.

Group 2 includes cements that show the lightest $\delta^{18}O$ values, from −14 ‰VPDB to −8 ‰VPDB, which are up to 10 ‰VPDB lighter than their correspondent host rocks (Figs. 7 and 8b). These cements have $^{87}Sr/^{86}Sr$ ratios between 0.7074 and 0.7080 (Fig. 8a–b), and $\delta^{13}C$ between −12 ‰VPDB and +2 ‰VPDB, which may either be similar or lighter than those values of their adjacent host rocks (Fig. 7). Additionally, comparing all cements, calcites from Group 2 exhibit low to intermediate Sr contents (between 390 and 2000 ppm), intermediate Mn contents (less than 700 ppm), and intermediate Y/Ho ratios (between 40 and 80) (Fig. 9a–c). All these calcite cements precipitated in large-scale faults and related fractures affecting different sectors of the Bóixols-Sant Corneli anticline. Eleven representative clumped isotope measurements of Group 2 cements were completed with 4 previously reported measurements in the area (Muñoz-López et al., 2020b; Nardini et al., 2019) to reconstruct the temperature and composition of the precipitating fluids. Obtained Δ_{47} values range from 0.413 ± 0.009 to 0.529 ± 0.009, which correspond to precipitation temperatures ranging from 50 to 110 °C and $\delta^{18}O_{fluid}$ varying from −4.3 to +4.2 ‰SMOW.

Group 3 of calcites (Figs. 7–9) includes cements characterized by a narrow range of the $\delta^{18}O$ values, between −8 and −6‰ VPDB (Figs. 7 and 8b), and $\delta^{13}C$-depleted values, between −10 and + 2‰ VPDB, which are up to 10‰ VPDB lighter than their surrounding host rocks (Fig. 7). The $^{87}Sr/^{86}Sr$ ratios of these calcites, between 0.7073 and

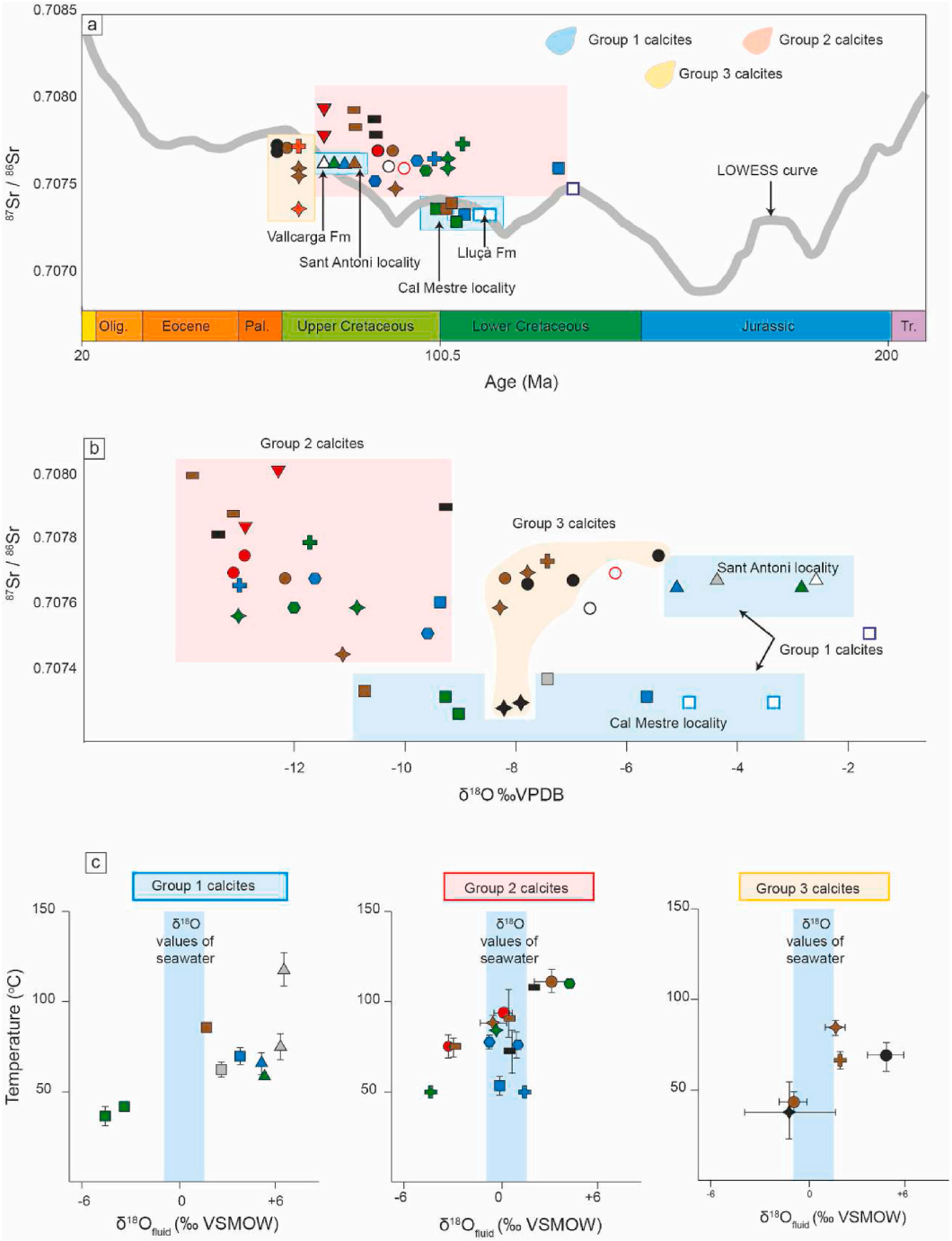

Fig. 8. (a) $^{87}Sr/^{86}Sr$ ratios of the three groups of calcites compared with the $^{87}Sr/^{86}Sr$ ratios of seawater trough time from the LOWESS curve (thick grey line) (McArthur et al., 2012). (b) $^{87}Sr/^{86}Sr$ ratio plotted against the $\delta^{18}O$ values. (c) The temperature (T) of precipitation and the $\delta^{18}O_{fluid}$ calculated from clumped isotope thermometry. Symbol and color key in Fig. 7 and 9. (For interpretation of the references to color in this figure legend, the reader is referred to the Web version of this article.)

0.7077, are lower than values of their correspondent host rocks but within the range of Cretaceous carbonates, which range between 0.7072 and 0.7079, approximately (McArthur et al., 2012) (Fig. 8a–b). Finally, these cements display the lowest Sr contents (less than 500 ppm) and Y/Ho ratios (less than 60) (Fig. 9). Cements from Group 3 precipitated in centimetric to metric-scale fractures in the backlimb (Sant Joan locality) and forelimb (Coll de Nargó and Forat de Bóixols localities) of the Bóixols-Sant Corneli anticline. The previous contributions of (Muñoz-López et al., 2020b; Nardini et al., 2019) also reported the temperature of precipitation and composition of the parent fluids for four cements from Group 3 and these data has been complemented with a new clumped isotope measurement. Obtained Δ_{47} values range from 0.494 ± 0.016 to 0.646 ± 0.009, which correspond to precipitation temperatures ranging from 40 to 85 °C and $\delta^{18}O_{fluid}$ varying from −1.3 to +4.8 ‰SMOW.

5. U–Pb geochronology of fracture-filling calcite cements

Twenty-three ages were obtained for different fracture-filling calcite cements (Fig. 10), varying from Late Cretaceous (79.8 ± 1.2 Ma) to late

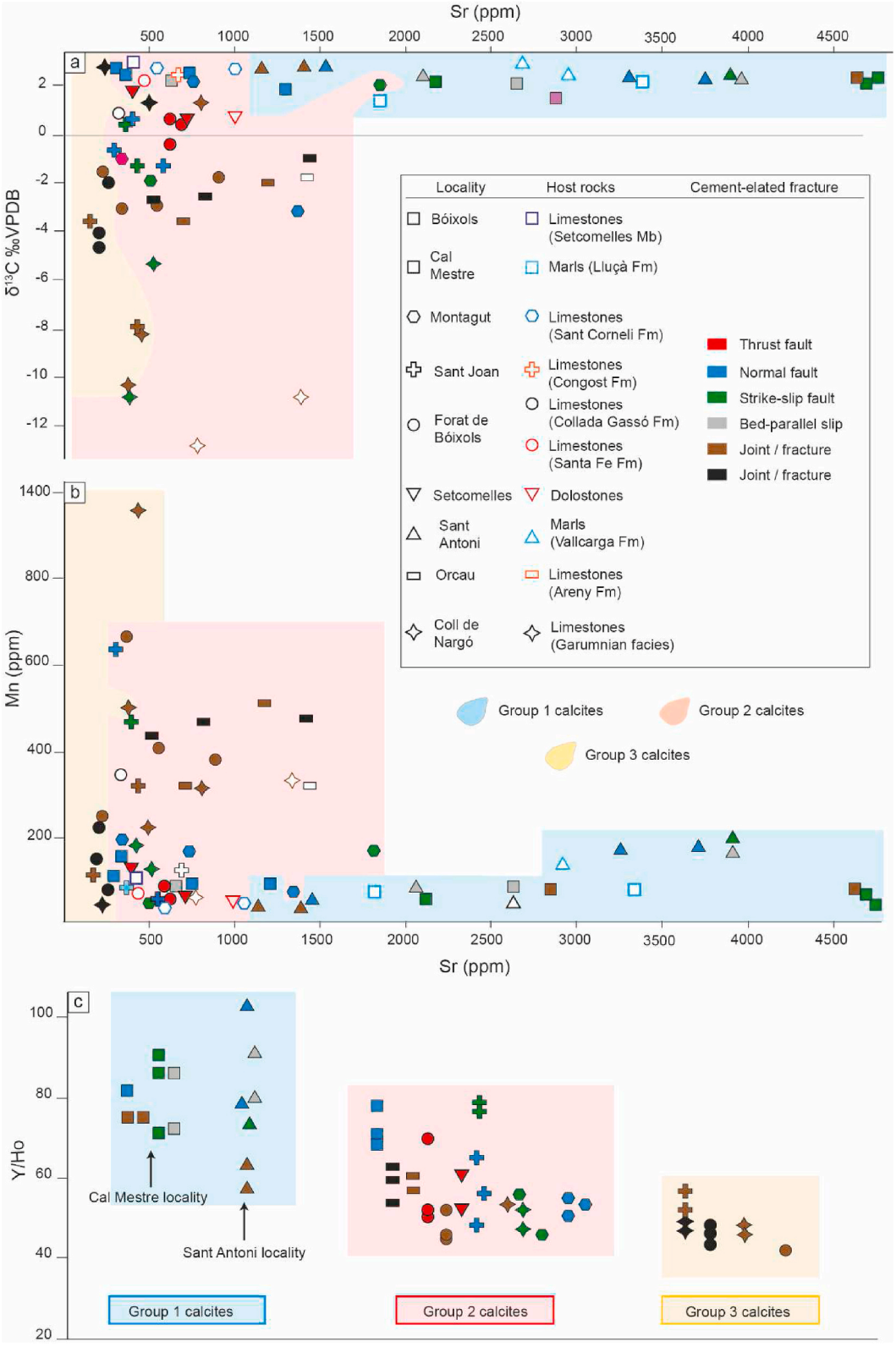

Fig. 9. Elemental composition of the three groups of calcites and their associated host rocks. (a) Sr content vs $\delta^{13}C$ values. (b) Mn content vs Sr content. (c) Y/Ho ratio.

Miocene (9.0 ± 4.6 Ma). These U–Pb ages were acquired for calcite cements from Group 2 (18 out of 23), which precipitated along the Bóixols thrust, the Montagut fault system and other large faults affecting the entire anticline (Fig. 10), and for cements from Group 1 (3 out of 23) and from Group 3 (2 out of 23). These results together with eight previously published dates (Cruset et al., 2020a,b; Haines, 2008) provide a well constrained absolute timing of deformation and fluid flow in the frontal anticline of the Bóixols thrust sheet (Fig. 10).

Calcite cements and clay minerals were dated in the Bóixols thrust in Setcomelles, Forat de Bóixols and Abella de la Conca localities. At

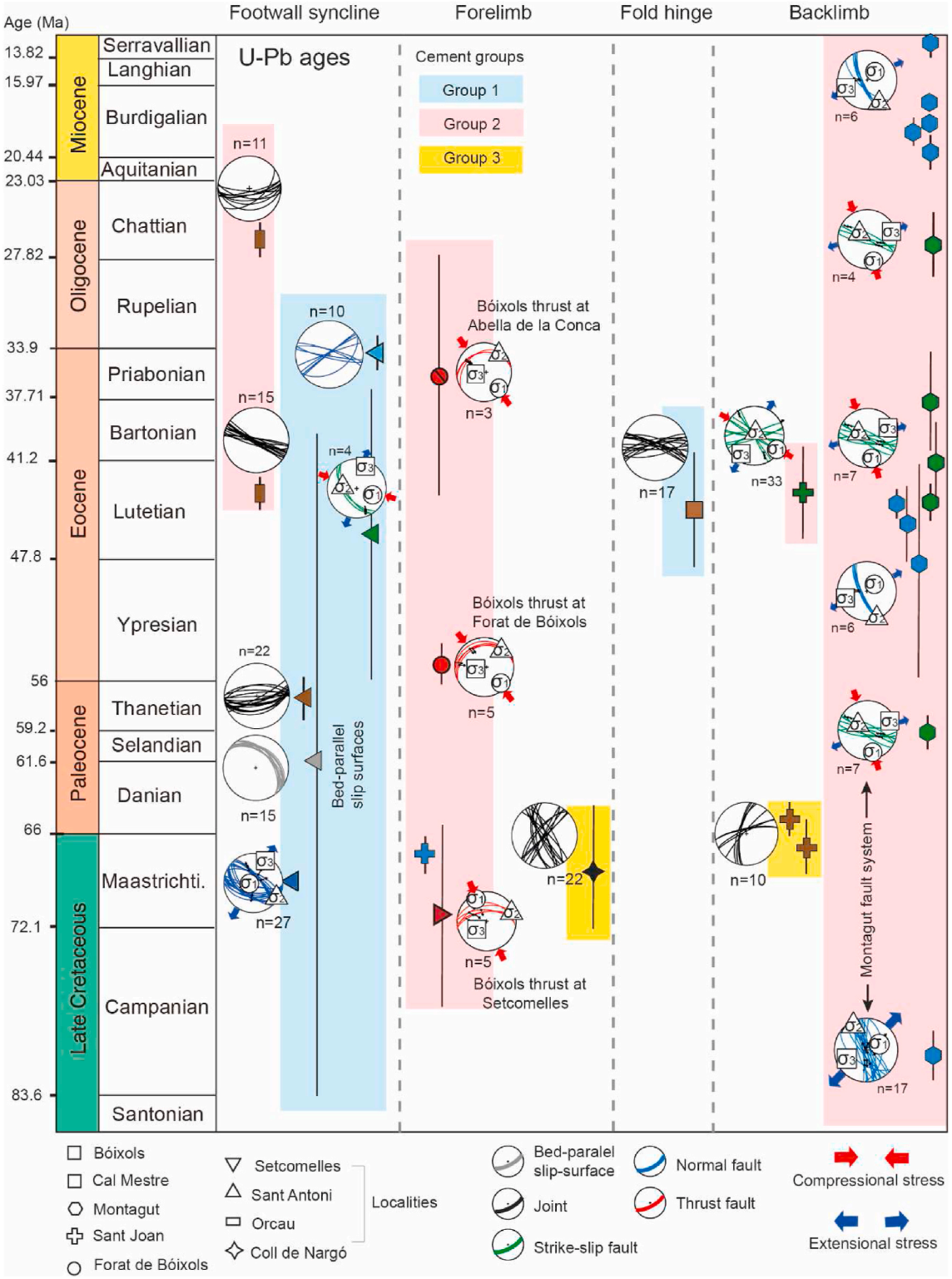

Fig. 10. Sequence of fracturing and absolute ages of the successive calcite cementation phases in the Bóixols-Sant Corneli anticline as constrained by fracture analysis and U–Pb geochronology of vein cements. The lower-hemisphere equal-area projections are also arranged according to the structural position of the anticline. Dated cements are grouped according to the three geochemical groups.

Setcomelles, previously Ar–Ar dating of clays sampled in a fault core, yielded an age of 71.2 ± 6.4 Ma (Haines, 2008), whereas an U–Pb age of 55.5 ± 1.2 Ma was obtained at Forat de Bóixols (Cruset et al., 2020b). Both dates are older than the new U–Pb age reported in this study for the Bóixols thrust at Abella de la Conca (36.6 ± 7.9 Ma).

In the several faults that constitute the Montagut fault system, which affect the Upper Cretaceous pre-orogenic sequence at the Montagut locality, we obtained 13 U–Pb dates. These dates present important age variations from the oldest one during the Late Cretaceous at 79.8 ± 1.2 Ma to the youngest one during the late Miocene at 9.0 ± 4.6 Ma. Using this dataset, which has been completed with two previously published dates of the area, we report the formation and/or reactivation of normal

faults and related fluid flow at 79.8 ± 1.2 Ma, 48.8 ± 8.6 Ma to 43.9 ± 0.7 Ma, 20.8 ± 1.2 Ma to 16.8 ± 0.2 Ma and 9.0 ± 4.6 Ma (Fig. 10). Therefore, the Late Cretaceous date (79.8 ± 1.2 Ma) is: (i) the oldest obtained age in this contribution and, (ii) older than the first age documented for the Bóixols thrust (71.2 ± 6.4 Ma, Haines, 2008). Ages for the Organyà fault and other pre-orogeny fractures were not obtained in this study. In the same way, at the Montagut locality, we document the formation and/or reactivation of strike-slip faults during precipitation of calcite cements at 58.7 ± 1.1 Ma, 45.5 ± 0.8 Ma to 37.8 ± 3.5 Ma and 27.6 ± 2.3 Ma. The precipitation of calcite cement in strike-slip faults during the Lutetian, coincides with the formation of similar strike-slip faults in other localities, according to the age of their related cements at 43.4 ± 3.0 Ma (Sant Joan locality) and 45.7 ± 9.7 (Sant Antoni locality).

At the Sant Joan locality, we did not obtain ages for the Sant Joan fault system. However, we measured two dates for calcite veins at 67.1 ± 2.2 Ma and 65.4 ± 1.3 Ma, which precipitated in metric fractures in this locality. The former age has a mean squared weighted deviate (MSWD) of 10.6. As this value is higher than 2, it could indicate a mixing of ages, an open system, or an incomplete initial equilibration of the Pb isotopes (Rasbury and Cole, 2009).

Other obtained ages in the Bóixols-Sant Corneli anticline account for the background deformation represented by fracture systems at different scales and studied at distinct localities. In this line, we document the formation of layer-parallel slip surfaces at 61.0 ± 21.8 Ma in Cal Mestre Locality. Similarly, we also report the formation and/or reactivation of meter-scale fractures during the Late Cretaceous to Oligocene, according to precipitation of calcite cements at 67.9 ± 3.9 Ma, 56.9 ± 1.4 Ma, 44.7 ± 4 Ma to 43.9 ± 1.0 Ma and 27.4 ± 0.9 Ma (Fig. 10).

6. Discussion

6.1. Sequence of deformation and age and duration of fold evolution

In this section we stablish the sequence of fracturing based on field data and structural observations and provide absolute age constraints from the U–Pb dating of calcite veins in the Bóixols-Sant Corneli anticline.

Firstly, we use relative chronological relationships to determine whether the studied fracture and fault systems developed prior, during or after the main folding stage. It must be highlighted that fractures in the Bóixols-Sant Corneli anticline are controlled by the presence of inherited extensional structures, resulting in fractures that do not preserve a symmetrical orientation with respect to the local fold axis (Nardini et al., 2019; Shackleton et al., 2011; Tavani et al., 2011). Therefore, the approaches used to determine the relative age of fracture development are: (i) the crosscutting relationships between different fracture and striae sets; (ii) the relation between fracture orientation and bedding attitude; and (iii) the restriction of fractures to specific pre- and/or syn-orogenic units. Following these assumptions, we summarize the fold evolution in four stages of deformation, which are in line with previous studies describing the evolution of folds in fold-and-thrust belts (Amrouch et al., 2010; Beaudoin et al., 2015, 2020; Casini et al., 2011; Lacombe et al., 2021; Tavani et al., 2015):

Pre-orogenic extension: the WNW-ESE to NNW-SSE normal faults in the Bóixols and Cal Mestre localities only affect pre- and syn-rift (pre-orogenic) units and are consistent with the NNE-SSW extensional regime that predates the Pyrenean compression (Berástegui et al., 1990). Accordingly, these faults have previously been associated with an Early Cretaceous rifting in the area (Berástegui et al., 1990; García-Senz, 2002).

Layer-parallel shortening and subsequent folding stage: during the emplacement of the Bóixols thrust sheet and growth of the Bóixols-Sant Corneli anticline, slip directions provided by fault orientations and related slickenlines are consistent with a N–S to NNW-SSE shortening direction (Fig. 10), which agrees with the regional tectonic transport direction in the Pyrenees (Choukroune, 1989; Macchiavelli et al., 2017; Srivastava et al., 1990). The estimated stress field calculated for the emplacement of the Bóixols thrust evidences a SSE transport direction, compatible with the estimated N–S to NNW-SSE shortening direction, and a subhorizontal maximum principal stress. The orientation of the conjugate NNW-SSE and NNE-SSW fracture sets, showing a subhorizontal σ_1, is compatible with the shortening direction reported for the Bóixols thrust (Fig. 10), and the similar petrographic and geochemical features of the calcite cements found within these conjugate fractures and the Bóixols thrust accounts for a synchronous development. Besides, opening fractures with similar NNW-SSE orientations developed during successive fracturing events, as evidenced by cross-cutting relationships between their associated vein cements (e.g., Fig. 6e). These opening fractures likely developed with a horizontal least compressive principal stress and thus, during compression (Anderson, 1951). Previous studies already reported the formation of NNW-SSE to NNE-SSW fractures during the main folding stage in the western termination of the Bóixols-Sant Corneli anticline (Shackleton et al., 2011). These NNW-SSE to NNE-SSW fracture orientations have been interpreted as controlled by the regional shortening direction and by inherited extensional structures, respectively (Tavani et al., 2011).

Other deformation structures, interpreted as developed during the layer parallel shortening and main folding stages include the formation of bed-parallel slip surfaces across the fold, which is indicative of flexural-slip commonly associated with the main folding stage (Tavani et al., 2011, 2017) as well as the strike-slip reactivation of inherited extensional faults that developed during the pre-orogenic deformation. This reactivation, which is supported by the presence of overprinting striae sets exhibiting oblique-slip and strike-slip kinematics and by the coexistence of two calcite cements in the same fractures, was likely caused due to their favorable orientation with respect to the shortening direction during inversion. In the same way, fractures exhibiting an E-W orientation that is parallel to the fold axis have been associated with local extension due to strata bending, as interpreted other anticlines elsewhere (Beaudoin et al., 2015).

Fold tightening stage: this late deformation stage is represented by fractures that are still consistent with a NNW-SSE shortening direction but are characterized by a constant orientation independently of the bedding dips, and by large faults offsetting the already folded beds of the anticline. These features are indicative of a fold tightening stage (Amrouch et al., 2010; Beaudoin et al., 2020; Casini et al., 2011; Lacombe et al., 2021; Tavani et al., 2015). At this stage, the ongoing shortening is expected to be oriented at a high angle with respect to bedding and the resulting deformation has been interpreted as accommodated by: (i) the formation of thrust faults (Bóixols thrust in the Forat de Bóixols and the Abella de la Conca localities), offsetting the steeply dipping forelimb of the anticline; and (ii) strike-slip faults exhibiting subhorizontal striae sets and recording a subhorizontal maximum principal stress regardless of the bedding dips across the anticline (Fig. 10).

Post-folding normal faulting: normal faults displace already folded beds in the backlimb of the anticline (the Sant Joan fault system and subsidiary faults around the Montagut fault system) in the Sant Joan and Montagut localities, respectively. As this extensional faulting postdate strata tilting, these faults have been attributed to a post-folding extensional stage that could be associated with the collapse of the Bóixols-Sant Corneli structure (Mencos, 2010). As reported in other areas elsewhere, positive uplift may induce gravity-driven extension that mainly affects the limbs of anticlines (Morley, 2007; Tavani et al., 2014, 2015).

Beyond this, U–Pb chronology of the successive vein cements allowed us to refine the absolute timing of vein development, which is in line with the sequence of deformation interpreted from the structural analysis, and to link the four deformation stages in the Bóixols-Sant Corneli anticline with the regional deformation of the Bóixols thrust sheet during the evolution of the South-Central Pyrenees. The collected samples of the normal faults interpreted as pre-orogenic deformation

have not given measurable ages. Thereby, we provide absolute U–Pb age constraints for the layer parallel shortening and subsequent folding stage, for the late stage of fold tightening and for the post-folding normal faulting, as summarized below.

The succession of U–Pb ages measured in calcite veins that precipitated in fractures attributed to the layer-parallel shortening and subsequent folding stages range from 71.2 ± 6.4 to 56.9 ± 1.4 Ma (Fig. 10). These ages are coeval with the upper Santonian to Paleocene growth strata deposition along the southern flank of the Bóixols-Sant Corneli anticline. Thus, corroborating the formation of: (i) conjugated NNW-SSE and NNE-SSW fracture sets, (ii) bed-parallel slip surfaces across the fold, (iii) E-W bed-perpendicular fractures trending parallel to the fold axis, and (iv) strike-slip reactivation of inherited extensional faults, during the emplacement of the Bóixols thrust sheet and growth of the Bóixols-Sant Corneli anticline along its front during Late Cretaceous to Paleocene times. This is also consistent with previous estimates placing the emplacement of the Bóixols trust sheet and its eastern equivalent structure, the Upper Pedraforca thrust sheet, from 70.6 ± 0.9 to 55.3 ± 0.5 Ma (Cruset et al., 2020b).

Additionally, a sample from the NNW-SSE Montagut fault system, in the region of relay between the anticlines of Bóixols and Sant Corneli, has given an age of 79.8 ± 1.2 Ma (middle Campanian). This age is the oldest associated with a normal fault in the study region and therefore synchronous with the well-preserved Late Cretaceous growth strata deposits at the SW end of the Sant Corneli anticline. Indeed, NW-SE normal faults have also been observed deforming Upper Cretaceous syn-orogenic sediments in the Sant Antoni locality, in the western end of the Bóixols-Sant Corneli anticline. The formation of the former NNW-SSE normal faults is consistent with the formation of extensional structures oriented parallel to the shortening direction (Tavani et al., 2011). The development of the later NW-SE faults is consistent tectonic instability and basin margin collapse during the emplacement of the Bóixols thrust and the initial stages of fold growth (Bond and McClay, 1995; Guillaume et al., 2008; Shackleton et al., 2011).

The U–Pb ages ranging from 55.5 ± 1.2 to 27.4 ± 0.9 Ma postdate the upper Santonian to Paleocene growth strata that fossilizes the Bóixols structure (Fig. 10). This corroborates the formation of thrust faults offsetting the forelimb of the anticline (Bóixols thrust in the Forat de Bóixols and the Abella de la Conca localities) and strike-slip faults across the fold during the tightening of the Bóixols thrust sheet including its frontal Bóixols-Sant Corneli anticline in Eocene and Oligocene times. This fold tightening is therefore coeval with the tectonic transport of the Bóixols thrust sheet to the south over the basal thrust of the South-Central Pyrenean Unit during a period that is characterized by maximum shortening rates (Cruset et al., 2020b; Grool et al., 2018; Vergés et al., 2002). During this period, we also report the formation and/reactivation of NNW-SSE normal faults, NW-SE strike slip faults and E-W to WNW-ESE opening veins, suggesting that these structures successively developed during the entire folding event (Fig. 10).

U–Pb dating of normal faults interpreted as post-folding structures reveals their formation at 20.8 ± 1.2 to 9.0 ± 4.6 Ma (Fig. 10). Coeval deformation has been documented in the SE Pyrenean thrust sheets through the reactivation of thrust faults and the growth of collapse normal faults dated by means of U–Pb geochronology (Cruset et al., 2020b).

To sum up, we interpret the evolution of fractures in the study area as a record of the pre-orogenic deformation, developed previously to 79.8 ± 1.2 Ma (Fig. 11). Our data also reveal the layer parallel shortening and subsequent folding stages, which lasted at least from 71.2 ± 6.4 to 56.9 ± 1.4 Ma, during the emplacement of the Bóixols thrust sheet and growth of the Bóixols-Sant Corneli anticline along its front (Fig. 11). The late stage of fold tightening from 55.5 ± 1.2 to 27.4 ± 0.9 Ma, coeval with the tectonic transport of the Bóixols thrust sheet to the south over the South-Central Pyrenean Unit basal thrust. Therefore, the absolute dating of mesostructures presented in this study not only corroborates the sequence of deformation interpreted from the field and structural data but also allowed us to provide new constraints on the age and duration of the entire folding event (Lacombe et al., 2021). Thus, we suggest that the layer parallel shortening and folding substages lasted for about 14 Myr, whereas the late fold tightening had a duration of about 28 Myr. This indicates that the entire folding event lasted at least 42 Myr (Fig. 11). These interpretations are in line with recent studies estimating the duration of fold growth in the Pyrenees and elsewhere using direct dating of vein cements (Lacombe et al., 2021).

Besides, it is worth nothing that this study evidences the continuous formation of similar fracture and fault systems throughout the folding process. Likewise, we report the precipitation of calcite cements with similar petrographic and geochemical features that developed during different deformation stages. Therefore, we conclude that without the absolute timing constraints provided by U–Pb geochronology, different fractures and different fluid flow events that occurred in the several stages of fold evolution would potentially be interpreted as occurred

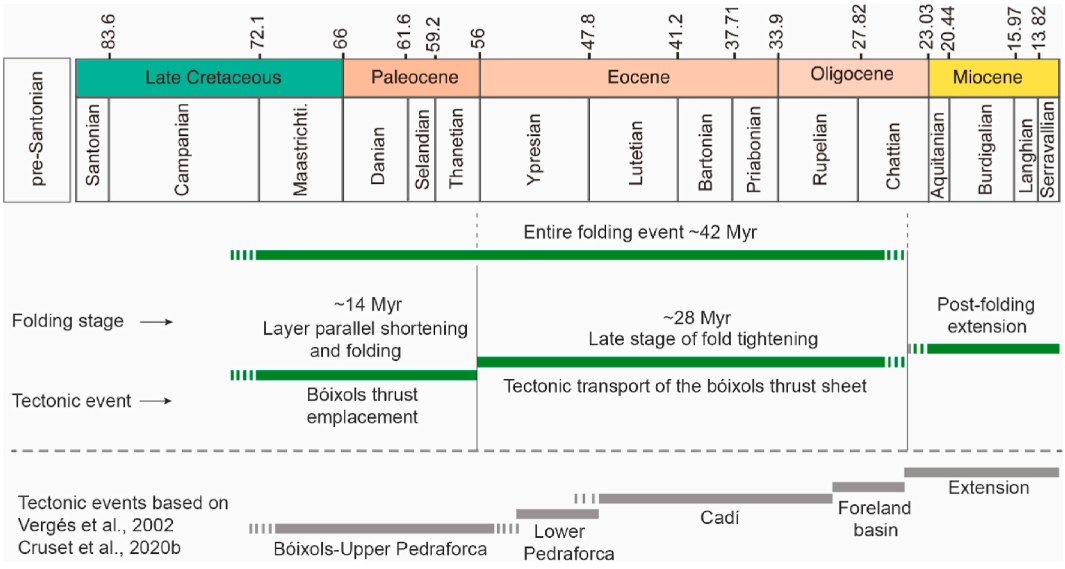

Fig. 11. Age and duration of fold evolution in the Bóixols-Sant Corneli anticline and comparison with the regional deformation of the Bóixols thrust sheet during the evolution of the Southern Pyrenees.

coevally during the same substage of folding. This, therefore, has important implications for the prediction of fracture development and associated fluid flow migrations.

6.2. Open vs closed fluid behavior and relative extent of fluid-rock interactions

The presence of different calcite vein generations developed during the structural evolution of the study area, as well as the wide range of U–Pb ages and isotopic and elemental composition of the vein cements, evidence a complex evolution of the fluid system throughout the entire deformation history.

In the Cal Mestre and Sant Antoni localities, present in the hinge of the Bóixols-Sant Corneli anticline and in the base of the syn-orogenic deposits in the footwall of the Bóixols thrust sheet, respectively, the calcite cements associated with successive episodes of fracturing and vein formation (i.e., Group 1 calcites) do not record significant changes in the cement composition through time (Figs. 7–9). Accordingly, all cements from this Group 1 have similar $\delta^{13}C$ values to their associated carbonate host rocks (Lluçà and Vallcarga Formations, respectively), which in turn yield typical marine values (Fig. 7) (Veizer et al., 1999). The $^{87}Sr/^{86}Sr$ ratios of the vein cements are similar to those ratios of local host rocks, which also reflect the composition of contemporaneous seawater (LOWESS curve in Fig. 8a). Indeed, the low Mn content of calcites Group 1 and related host rocks, responsible for their dark to non-luminescence, together with their high Sr content (Fig. 9a–b) and high Y/Ho ratios (Fig. 9c), reveal to be close to the elemental composition of marine carbonates derived from well-oxygenated seawater (Popp et al., 1986). Therefore, the similar petrographic and geochemical features of all calcite cements and host rocks from Cal Mestre and Sant Antoni localities indicate very low water-rock ratios (i.e., diffusive flow) and precipitation of successive calcite cements in a relatively closed/rock-buffered system during different fracturing events (Boutoux et al., 2014; Hurai et al., 2015; Vandeginste et al., 2012). In this scenario, the slight $\delta^{18}O$-depletion of calcites Group 1 (Fig. 7a), with respect to host rocks and typical marine values, indicates variation in fluid temperatures, from 36 and up to 116 °C, and locally in the fluid composition, from −4.7 to +6.5 ‰SMOW, during different events of calcite cement precipitation, as revealed by clumped isotope data. Variations in temperature are expected during different stages of deformation linked to the emplacement of the Bóixols thrust and growth of the Bóixols-Sant Corneli anticline. In contrast, the positive $\delta^{18}O_{fluid}$-values, measured in most calcites from Group 1 (Fig. 8c), indicate the presence of formation waters, which is consistent with a scenario mainly involving evolved marine fluids likely trapped in the surrounding Lower Cretaceous and Upper Cretaceous marine carbonates present in Cal Mestre and Sant Antoni localities, respectively. Locally, the negative $\delta^{18}O_{fluid}$-values, measured in two cements from Group 1 (Fig. 8c), likely indicate the infiltration of meteoric waters during the main folding and late fold tightening stages (Fig. 10). However, the similar isotopic and elemental signature between these two cements, the other cements from Group 1 and the adjacent marine host rocks indicate that the fluids precipitating in these veins migrated at relative low rates to equilibrate with the adjacent sedimentary formations. Therefore, we suggest that calcites Group 1 precipitated from formation, likely marine-derived fluids, and locally from meteoric waters, the composition of which was buffered by the adjacent Cretaceous marine carbonates.

The geochemical data of calcite cements from Group 2, precipitated in decametric to kilometric faults (the Bóixols thrust, the Montagut fault system, the Sant Joan fault system) and related fractures, evidence a different scenario than that of Group 1 cements. Calcites from Group 2 generally display the more depleted $\delta^{18}O$ values with respect to those of Group 1 and exhibit up to 10 ‰VPDB lighter values than their adjacent host rocks (Fig. 7). This $\delta^{18}O$-depletion is related to the relative high temperature of precipitation, up to 120 °C, suggesting that the fluids precipitating calcites Group 2 migrated rapid enough through fault zones to avoid efficient isotopic equilibration with surrounding host rocks (Beaudoin et al., 2011). On the other hand, the scattered $\delta^{13}C$ and $^{87}Sr/^{86}Sr$ ratios of Group 2 cements (Figs. 7–8), their variable enrichment in Mn contents (Fig. 9b), and their differing luminescence characteristics could indicate that the precipitating fluids had distinct fluid origins (marine, connate and/or meteoric) and that they interacted with different sedimentary units (Travé et al., 2007; Vandeginste et al., 2012). The variable origin of the precipitating fluids is recorded in the $\delta^{18}O_{fluid}$, which yield values, between −4.4 and + 4.3 ‰SMOW, that is between the range of meteoric, marine and formation waters. Similarly, the Y/Ho ratios of Group 2 of cements indicate a variable degree of siliciclastic and marine influence (Fig. 9c). As large-scale faults affect all stratigraphic sequences involved in the anticline, from Jurassic marine to Paleocene continental host rocks, such variation may result from the interaction between the vein-forming fluids and marine (high Y/Ho ratio) or continental (low Y/Ho ratio) rocks (Bau, 1994; Nardini et al., 2019). Accordingly, we interpret that calcites from Group 2 precipitated from fluids that did not equilibrated geochemically with the host rocks. As this group mainly concerns large faults and related fractures such as the Bóixols thrust, the Montagut fault system, the Sant Joan fault system, among others, these large fractures acted as efficient conduits for fluid migration during their formation at different stages of the deformation history.

Cements from Group 3 precipitated in centimetric to metric scale fractures in the limbs of the Bóixols-Sant Corneli anticline, where Upper Cretaceous post-rift (pre-orogenic) marine carbonates are widely exposed. The isotopic signature of these cements, ranging between −8 and −6 ‰VPDB for $\delta^{18}O$ and between −10 and + 2 ‰VPDB for $\delta^{13}C$, fall within the range of meteoric carbonates (Pujalte et al., 2009; Travé et al., 2007; Veizer, 2005), although with varying influence of the marine host rocks as evidenced by the positive $\delta^{13}C$ values of some cements (Fig. 7). The meteoric origin of cements from Group 3 is supported by their $^{87}Sr/^{86}Sr$ ratios, which are lower than those values of their adjacent host rocks (Fig. 8a), and by the elemental composition of these cements, yielding the lowest Sr contents with respect to other cements and host rocks. The low Y/Ho ratios, which indicates the influence of terrigenous sediments (Bau, 1994), and their common CL zonation (Fig. 6), which points to oxidizing-reducing fluctuations, are again characteristic features of the meteoric environment. At outcrop scale, clumped isotopes reveal a progressive increase in precipitation temperatures, from 40 °C to 80 °C (Forat de Bóixols locality) and from 25 °C to 85 °C approximately (Coll de Nargó locality), as well as an enrichment in $\delta^{18}O_{fluid}$, from −1.8 to +5.9 ‰VSMOW and from −4.2 to +2 ‰VSMOW, respectively (Fig. 8c). This fact indicates a continuous shift in the fluid composition, from meteoric to evolved meteoric fluids due to water-rock interactions at increasing temperatures during deformation. Therefore, these geochemical features indicate that the fluid system associated with metric fractures that developed in the limbs of the anticline, was open to the input of meteoric fluids, which geochemistry was influenced by the surrounding Upper Cretaceous marine carbonates.

6.3. Spatio-temporal variation of fluids across the Bóixols-Sant Corneli anticline

In this section, we discuss the distribution and variations of fluids in the distinct structural positions of the Bóixols-Sant Corneli anticline.

The host-rock buffered fluids from which calcites Group 1 precipitated characterizes the paleohydrological system in the hinge of the Bóixols-Sant Corneli anticline and in the base of the syn-orogenic deposits along the southern flank of the fold, where Cal Mestre and Sant Antoni localities are located, respectively (Fig. 12). In the hinge of the anticline (Cal Mestre locality), the Lower Cretaceous mudstones and marls from the Lluçà Formation have a minimum thickness of 2500 m (Lanaja, 1987). Due to the expected non-permeable character of this unit and its considerable thickness, the small-scale fractures (up to several

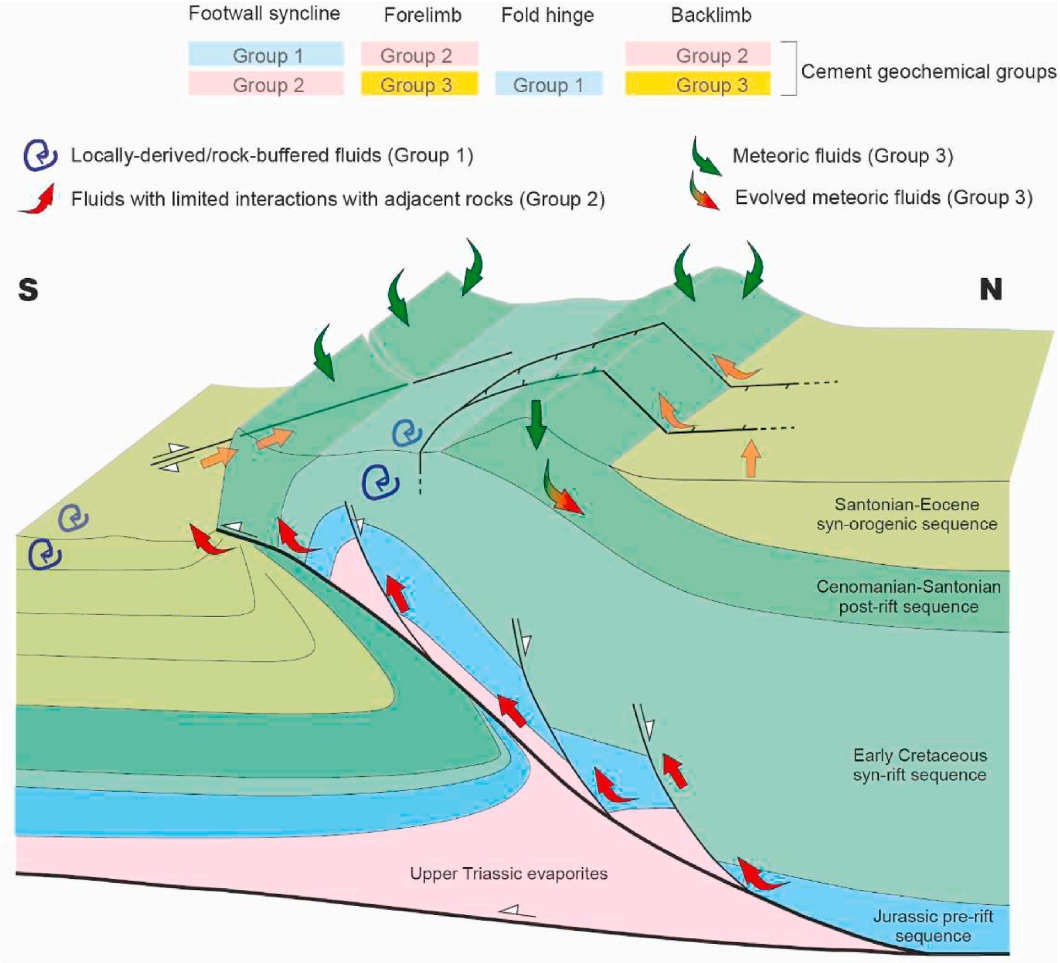

Fig. 12. Schematic cross-section (not to scale) of the Bóixols-Sant Corneli anticline along the front of the Bóixols thrust sheet showing the spatial variation of fluids in the several structural positions of this fold. Cross-section based on Vergés (1993).

meters long) occurring in this locality, likely represented poorly efficient conduits to connect different hydro-stratigraphic reservoirs and to prevent isotopic equilibration between fluids and host rocks. A similar rock-buffered fluid behavior has been observed in the core of the el Guix anticline in the Ebro foreland basin, where the $\delta^{13}C$ and $\delta^{18}O$ values of fracture-filling calcites are in geochemical equilibrium with their adjacent host carbonates (Travé et al., 2000). Contrarily, in the crestal and shallower domains of anticlines, the fluid system is often the opposite. Examples of this are the Puig-reig anticline, also in the Ebro foreland basin, and the Pico del Águila anticline in the Sierras Exteriores (Beaudoin et al., 2015; Cruset et al., 2016). These authors concluded that large faults and well-connected fracture networks that developed in response to outer arc extension at fold hinges during fold growth facilitated the opening of the fluid system and the percolation of meteoric fluids in disequilibrium with their adjacent host rocks. These observations, together with that of this study, reveal the compartmentalization of fold structures during deformation.

In the base of the syn-orogenic deposits (Sant Antoni locality), the Upper Cretaceous marine mudstones from the Vallcarga Formation were deposited during the early contraction and initial growth of the Bóixols-Sant Corneli anticline (Ardèvol et al., 2000). Therefore, the local origin of the fluids in this domain is consistent with the marine setting of deformation that likely affected recently deposited and poorly lithified sediments (Travé et al., 2007).

Fluids with limited geochemical interactions with adjacent host rocks from which calcites Group 2 precipitated characterize the fluid system associated with large-scale faults and related fractures, which affect the different structural and stratigraphic positions of the Bóixols-Sant Corneli anticline and developed throughout its whole deformation history (Fig. 12). The development of these large fracture systems facilitated the transfer of fluids between different hydro-stratigraphic units decreasing the extent of interaction between fluids and host rocks, as has already been documented in the frontal domain of the anticline. In this line, according to Nardini et al. (2019), large strike-slip faults from Coll de Nargó locality acted as transfer zones for the migration of deeper Late Cretaceous connate waters to shallower non-marine sediments of the Paleocene Garumnian facies. Likewise, the Bóixols thrust in Forat de Bóixols locality acted as an efficient longitudinal conduit for the migration of deep formation waters also derived from Cretaceous carbonates (Muñoz-López et al., 2020b). In both examples, these large faults enhanced connectivity between different sedimentary units, allowing heated formation fluids to migrate upward through fault zones with limited equilibration with adjacent rocks (Nardini et al., 2019; Muñoz-López et al., 2020b). These fluids were likely expelled due to vertical compaction linked to thrust sheet emplacement and/or tectonic horizontal shortening (squeegee-type fluid flow) during continuous compression (; Machel and Cavell, 1999; Oliver, 1986; Roure et al., 2010; Smeraglia et al., 2022; Sun et al., 2022; Travé et al., 1997, 1998; Vandeginste et al., 2012).

Finally, meteoric and evolved meteoric waters from which calcites Group 3 precipitated characterizes the fluid system in the limbs of the Bóixols-Sant Corneli anticline, where Forat the Bóixols, Coll de Nargó and Sant Joan localities are located (Fig. 12). Meteoric waters generally infiltrate at high structural reliefs such as the crestal domain of

anticlines (Beaudoin et al., 2015; Cruset et al., 2016). However, in the Bóixols-Sant Corneli anticline meteoric fluid percolation was mainly recorded in the fold limbs, and locally in the fold hinge, because most of the crestal domain was eroded synchronously with folding (Tavani et al., 2011). On the other hand, the geochemical and geochronological data of some calcite cements from Group 3 set the initial infiltration of meteoric fluids during the Maastrichtian, during formation of their related fractures at ca. 67–65 Ma (Fig. 10). This fluid flow event coincides with the transition from marine to continental conditions, during the progressive uplift of the structure, coevally with sedimentation of the non-marine continental Garumnian facies (Tremp Group) from Late Maastrichtian to Paleocene (Garcés et al., 2020; Plaziat, 1981). Therefore, the emersion of the Bóixols structure has been recorded by the fluids that migrated through fractures during deformation. This scenario of meteoric fluid infiltration during the main folding stage and during the change from marine to continental conditions have also been reported in other studies focused on the evolution of fold-fluid systems (Beaudoin et al., 2015; Evans and Fischer, 2012; Nardini et al., 2019; Travé et al., 1998, 2007).

In conclusion, our data reveal that the fluid flow history and the extent of fluid-rock interaction varied at the several structural positions of the Bóixols-Sant Corneli anticline and according to the age and nature of their stratigraphy and the involved fracture networks. This indicates a compartmentalization of the fluid system (Fig. 12). Thus, in the hinge of the fold, at least around Cal Mestre locality, and in the base of the syn-orogenic deposits (Sant Joan locality), the fluid system was locally derived and/or well equilibrated with the host rocks, revealing a high extent of fluid-rock interaction. These local/rock-buffered fluids were basically evolved marine and/or connate waters derived from the adjacent Lower Cretaceous and Upper Cretaceous marine carbonates, although influences of meteoric waters were also locally present. Contrarily, along large faults, affecting different parts of the anticline, and in the fold limbs, the paleohydrological system was different. Large faults acted as conduits for the migration of fluids with limited chemical interactions with adjacent host rocks, suggesting that these faults have been efficient conduits for upward fluid flow during their development in the Bóixols-Sant Corneli anticline. The fold limbs registered the infiltration and evolution of meteoric waters with varying degrees of fluid-rock interactions at increasing temperatures during deformation (Fig. 12). Therefore, our data suggest that in the studied anticline the relative scale and distribution of fracture networks together with the involved stratigraphy were the main controls on the source, the distribution of fluids and the degree of fluid-rock interactions during deformation.

6.4. Scale of fluid flow and comparison with other compressional settings

In this section, we evaluate the scale of fluid flow in rocks forming the Bóixols thrust sheet and compare our results with other Pyrenean structures and other worldwide compressional belts. The Bóixols thrust sheet corresponds to the uppermost and oldest emplaced structure of the southern-central Pyrenean cover thrust units. Therefore, the structural position of this thrust sheet, detached along the Upper Triassic evaporites and above Lower Triassic detrital sediments of the Buntsandstein and the Paleozoic basement, allows us to assess the possible input of external fluids derived from these three potential reservoirs. In a previous section, we concluded that advective fluid flow was linked to the presence of major fault zones (including the Bóixols thrust) and associated fractures, which acted as preferential fluid flow pathways. Therefore, the geochemical signature of calcite cements precipitated in these fractures (Group 2 calcites) provide evidence on the relative scale of fluid flow and the fluid circulation depth. Thus, during precipitation of Group 2 calcites, a maximum temperature of around 120 °C was obtained from clumped isotopes in calcites precipitated in fractures associated with the Bóixols thrust in Forat de Bóixols locality (Fig. 8c) (Muñoz-López et al., 2020b). Assuming a normal geothermal gradient of 30 °C/km (Travé et al., 2007), these temperatures would have been reached at 3–4 km depth. Considering the thickness of the Bóixols thrust sheet (around 5 km thick), such temperatures imply circulation of fluids along fault zones that were originated in the deeper parts of the sedimentary cover. Indeed, the $\delta^{18}O_{fluid}$ of this group of cements, yielding maximum values of +5.5 ‰VSMOW, indicate the presence of formation waters, as has been explained before, and discard the input of basement-related fluids such water derived from and/or equilibrated with metamorphic rocks (Sheppard, 1981). In the same way, the $^{87}Sr/^{86}Sr$ ratios of the vein cements documented in this study are (1) within the range of marine carbonates (LOWESS curve in Fig. 8a), (2) within the range of synkinematic veins precipitated in the sedimentary cover (i.e., $^{87}Sr/^{86}Sr < 0.710$) (Muñoz-López et al., 2020a), and (3) significantly lower than values of cements precipitated from fluids that have interacted with Triassic evaporites or with Paleozoic basement rocks (Muñoz-López et al., 2020a). All these observations indicate that the fluid system in the study area was restricted to the scale of the Bóixols thrust sheet and rule out the input of external fluids derived from the underlying Triassic detachment, from deeper cover units such as the Buntsandstein or from the Paleozoic basement. An exception arises for the cement precipitated in the Bóixols thrust-related deformation at the Setcomelles locality, which exhibits the most radiogenic $^{87}Sr/^{86}Sr$ ratio in this study, similar to Upper Triassic values (Fig. 8a). Therefore, fluids derived from Upper Triassic evaporites acting as a main detachment of the Bóixols thrust sheet could have locally infiltrated the paleohydrological system, as has also been reported in other salt-detached Pyrenean structures (Crognier et al., 2018; Cruset et al., 2020a; Lacroix et al., 2011; Travé et al., 2007).

The results presented in this study also reveal that the frontal anticline (the Bóixols-Sant Corneli anticline) of the Bóixols thrust sheet shares a common fluid flow behavior with other worldwide compressional structures above evaporitic detachments. In these structures, the paleohydrological system only involves fluids sourced above the detachment levels, which may act as a lower boundary for the fluid system, preventing the input of fluids from deeper parts of the compressional belt. This fluid flow scenario in the Bóixols thrust sheet is similar to that of: 1) worldwide detachment folds (Beaudoin et al., 2014); 2) other south Pyrenean structures detached in Triassic and Eocene evaporitic units such as the Pico del Águila and El Guix anticlines (Beaudoin et al., 2015; Travé et al., 2000), the Monte Perdido and Abocador thrusts (Cruset et al., 2018; Lacroix et al., 2011), and the Upper and Lower Pedraforca thrust sheets (Cruset et al., 2020a); 3) other worldwide detached structures such as the Sierra Madre Oriental (Fischer et al., 2009; Lefticariu et al., 2005) and the Central Appalachians (Evans et al., 2012). Contrarily, in the absence of evaporites, a previous study highlighted that the fluid system is open to migration of hydrothermal, likely basement-derived fluids into the overlaying sedimentary cover (Beaudoin et al., 2011).

7. Conclusions

Our field and analytical data allowed to date and to analyze the relationships between fluid flow and fold evolution across different structural domains of the Bóixols-Sant Corneli anticline as summarized below.

1. The successive fracture-filling calcite cements identified in the Bóixols-Sant Corneli anticline were assembled in three calcite groups according to petrological and geochemical data. Group 1 includes calcites with similar petrographic and geochemical features with respect to their host carbonates (i.e., non-luminescent calcite cements with $\delta^{13}C$ values and $^{87}Sr/^{86}Sr$ ratios typical of marine carbonates); Group 2 comprises calcites with the lightest $\delta^{18}O$ values, down to −14 ‰VPDB, and the highest temperature of precipitation (up to 120 °C); and Group 3 includes calcites with $\delta^{18}O$ from −8 to −6 ‰VPDB, $\delta^{13}C$ down to −10 ‰VPDB and the lowest Sr contents.

2. The geochemistry of Group 1 cements indicates an essentially closed and/or rock buffered fluid system in the Early Cretaceous sequence from the hinge of the Bóixols-Sant Corneli anticline and in the upper Santonian to middle Campanian syn-orogenic sequence along the footwall of the Bóixols thrust.
3. The geochemistry of Group 2 cements indicates an open fluid system along the Bóixols thrust, the Montagut and the Sant Joan fault systems evidencing that these large faults acted as conduits for the upward migration of formation fluids, which evolved from different fluid origins. Group 3 cements indicate the presence and evolution of meteoric waters in the limbs of the Bóixols-Sant Corneli anticline. Meteoric fluids likely infiltrated at high structural reliefs during fold growth.
4. Twenty-three new U–Pb dates were measured in different sets of fracture-filling calcite cements in the Bóixols-Sant Corneli anticline presenting a wide range of ages from Late Cretaceous at 79.8 ± 1.2 Ma to late Miocene at 9 ± 4.6 Ma. These age variations are in line with the sequence of deformation inferred from field and microstructural observations.
5. Ten U–Pb ages measured in calcites from fractures attributed to the layer-parallel shortening and subsequent folding stages range from 71.2 ± 6.4 to 56.9 ± 1.4 Ma, coeval with the upper Santonian to Paleocene growth strata deposition along the southern flank of the Bóixols-Sant Corneli anticline. This confirms the development of (i) conjugated NNW-SSE and NNE-SSW fracture sets, (ii) bed-parallel slip surfaces across the fold, (iii) E-W bed-perpendicular fractures trending parallel to the fold axis, and (iv) strike-slip reactivation of inherited extensional faults, during the emplacement of the Bóixols thrust sheet and growth of the Bóixols-Sant Corneli anticline along its front during Late Cretaceous to Paleocene times.
6. Fifteen ages that range from 55.5 ± 1.2 to 27.4 ± 0.9 Ma and measured in calcites from fractures that cut already folded beds indicate the late tightening of the Bóixols-Sant Corneli anticline during Eocene and Oligocene periods, coeval with the southern tectonic transport of the Bóixols thrust sheet in the hanging wall of the South-Central Pyrenean Unit.
7. The Miocene ages from 20.8 ± 1.2 to 9.0 ± 4.6 Ma from normal faults that displace already folded beds in the backlimb of the anticline have been attributed to a post-folding extensional stage that could be associated with the collapse of the Bóixols-Sant Corneli structure.
8. The U–Pb geochronology allowed us to calculate the entire duration of folding for ~42 Myr with layer parallel shortening and folding for about ~14 Myr, whereas its tightening lasted around 28 Myr.
9. The major Bóixols thrust, the Coll de Nargó strike-slip faults and the Montagut fault system acted as preferential pathways for the upwards migration of fluids during compression, whereas background fracturing registered the presence of formation fluids that highly interacted with their adjacent host rocks. The paleohydrological system in the Bóixols-Sant Corneli anticline was restricted above the thick Upper Triassic evaporitic detachment level and thus comparable to other detached fold and thrust belts as the Central Appalachians and Sierra Madre Oriental as good examples.

Declaration of competing interest

The authors declare that they have no known competing financial interests or personal relationships that could have appeared to influence the work reported in this paper.

Acknowledgements

We thank Olivier Lacombe and another anonymous referee for their constructive and detailed reviews, which helped improve the quality of the manuscript. We also thank the excellent editorial guidance of Juliette Lamarche and Massimo Zecchin. This research was carried out within the framework of the DGICYT Spanish project PGC2018-093903-B-C22 (Ministerio de Ciencia, Innovación y Universidades/Agencia Estatal de Investigación/10.13039/501100011033/Fondo Europeo de Desarrollo Regional, Unión Europea), the Grup Consolidat de Recerca "Geologia Sedimentària" (2017-SGR-824) and the Grup Consolidat de Recerca "Modelització Geodinàmica de la Litosfera" (2017SGR-847). This work was also partially funded by ALORBE project (PIE–CSIC–202030E310). The PhD research of DML is supported by the FPI2016 (BES-2016-077214) Spanish program from MINECO. DC acknowledges the Spanish Ministry of Science and Innovation for the "Juan de la Cierva Formación" fellowship FJC2020-043488-I AEI/10.113039/501100011033. We thank Luis Fernando Martínez for helping in the fieldwork during his master's degree at the Universitat de Barcelona. Carbon and oxygen isotopic analyses were carried out at the Centre Científics i Tecnològics of the Universitat de Barcelona. Strontium analyses were performed at the CAI de Geocronología y Geoquímica Isotópica of the Universidad Complutense de Madrid. The elemental composition was analyzed at the geochemistry facility labGEOTOP of Geosciences Barcelona (GEO3BCN–CSIC). U–Pb analyses were performed at the Frankfurt Isotope and Element Research Center (FIERCE) from the Goethe-University Frankfurt (Germany).

References

Alcalde, J., Marzán, I., Saura, E., Martí, D., Ayarza, P., Juhlin, C., Pérez-Estaún, A., Carbonell, R., 2014. 3D geological characterization of the Hontomín CO2 storage site, Spain: multidisciplinary approach from seismic, well-log and regional data. Tectonophysics 627, 6–25. https://doi.org/10.1016/j.tecto.2014.04.025.

Amrouch, K., Lacombe, O., Bellahsen, N., Daniel, J.-M., Callot, J.-P., 2010. Stress and strain patterns, kinematics and deformation mechanisms in a basement-cored anticline: sheep Mountain Anticline, Wyoming. Tectonics 29. https://doi.org/10.1029/2009TC002525 n /a-n/a.

Anderson, E.M., 1951. The Dynamics of Faulting andDyke Formation With Application to Britain. Oliver and Boyd, London.

Angelier, J., 1984. Tectonic analysis of fault slip data sets. J. Geophys. Res. 89(B7), 5835–5848. https://doi.org/10.1029/JB089iB07p05835.

Ardèvol, L., Klimowitz, J., Malagón, J., Nagtegaal, P.J.C., 2000. Depositional sequence response to foreland deformation in the upper Cretaceous of the Southern Pyrenees, Spain. AAPG (Am. Assoc. Pet. Geol.) Bull. 84, 566–588. https://doi.org/10.1306/c9ebce55-1735-11d7-8645000102c1865d.

Bachu, S., 2000. Sequestration of CO2 in geological media: criteria and approach for site selection in response to climate change. Energy Convers. Manag. 41, 953–970. https://doi.org/10.1016/S0196-8904(99)00149-1.

Barbier, M., Leprêtre, R., Callot, J.P., Gasparrini, M., Daniel, J.M., Hamon, Y., Lacombe, O., Floquet, M., 2012. Impact of fracture stratigraphy on the paleohydrogeology of the Madison Limestone in two basement-involved folds in the Bighorn basin, (Wyoming, USA). Tectonophysics 576–577, 116–132. https://doi.org/10.1016/j.tecto.2012.06.048.

Bau, M., 1994. Evolution of the yttrium-holmium systematics of seawater through time. Mineral. Mag. 58A, 61–62. https://doi.org/10.1180/minmag.1994.58a.1.35.

Beaudoin, N., Bellahsen, N., Lacombe, O., Emmanuel, L., 2011. Fracture-controlled paleohydrogeology in a basement-cored, fault-related fold: sheep Mountain Anticline, Wyoming, United States. G-cubed 12, 1–15. https://doi.org/10.1029/2010GC003494.

Beaudoin, N., Bellahsen, N., Lacombe, O., Emmanuel, L., Pironon, J., 2014. Crustal-scale fluid flow during the tectonic evolution of the Bighorn Basin (Wyoming, USA). Basin Res. 26, 403–435. https://doi.org/10.1111/bre.12032.

Beaudoin, N., Huyghe, D., Bellahsen, N., Lacombe, O., Emmanuel, L., Mouthereau, F., Ouanhnon, L., 2015. Fluid systems and fracture development during syn-depositional fold growth: an example from the Pico del Aguila anticline, Sierras Exteriores, southern Pyrenees, Spain. J. Struct. Geol. 70, 23–38. https://doi.org/10.1016/j.jsg.2014.11.003.

Beaudoin, N.E., Labeur, A., Lacombe, O., Koehn, D., Billi, A., Hoareau, G., Boyce, A., John, C.M., Marchegiano, M., Roberts, N.M., Millar, I.L., Claverie, F., Pecheyran, C., Callot, J.P., 2020. Regional-scale paleofluid system across the Tuscan Nappe-Umbria-Marche Apennine Ridge (northern Apennines) as revealed by mesostructural and isotopic analyses of stylolite-vein networks. Solid Earth 11, 1617–1641. https://doi.org/10.5194/se-11-1617-2020.

Benedicto, A., Abdelrazek, M., Ledru, P., Mackay, C., Kinar, D., 2021. Structural controls of uranium mineralization in the basement of the athabasca basin, Saskatchewan, Canada. Geofluids 2021. https://doi.org/10.1155/2021/3853468.

Berástegui, X., Garcia-Senz, J.M., Losantos, M., 1990. Tecto-sedimentary evolution of the Organya extensional basin (central south Pyrenean unit, Spain) during the Lower Cretaceous. Bull. Soc. Geol. France 6, 251–263. https://doi.org/10.2113/gssgfbull.vi.2.251.

Bergbauer, S., Pollard, D.D., 2004. A new conceptual fold-fracture model including prefolding joints, based on the Emigrant Gap anticline, Wyoming. Bull. Geol. Soc. Am. 116, 294–307. https://doi.org/10.1130/B25225.1.

Bond, R.M.G., McClay, K.R., 1995. Inversion of a lower cretaceous extensional basin, south central pyrenees, Spain. Geol. Soc. Spec. Publ. 88, 415–431. https://doi.org/10.1144/GSL.SP.1995.088.01.22.

Bons, P.D., Elburg, M.A., Gomez-Rivas, E., 2012. A review of the formation of tectonic veins and their microstructures. J. Struct. Geol. 43, 33–62. https://doi.org/10.1016/j.jsg.2012.07.005.

Boutoux, A., Verlaguet, A., Bellahsen, N., Lacombe, O., Villemant, B., Caron, B., Martin, E., Assayag, N., Cartigny, P., 2014. Fluid systems above basement shear zones during inversion of pre-orogenic sedimentary basins (External Crystalline Massifs, Western Alps). Lithos 206–207, 435–453. https://doi.org/10.1016/j.lithos.2014.07.005.

Brandes, C., Tanner, D.C., 2014. Fault-related folding: a review of kinematic models and their application. Earth Sci. Rev. 138, 352–370. https://doi.org/10.1016/j.earscirev.2014.06.008.

Callot, J.P., Breesch, L., Guilhaumou, N., Roure, F., Swennen, R., Vilasi, N., 2013. Paleo-fluids characterisation and fluid flow modelling along a regional transect in northern United Arab Emirates (UAE). Front. Earth Sci. 5, 177–201. https://doi.org/10.1007/978-3-642-30609-9_9.

Casini, G., Gillespie, P.A., Vergés, J., Romaire, I., Fernández, N., Casciello, E., Saura, E., Mehl, C., Homke, S., Embry, J.C., Aghajari, L., Hunt, D.W., 2011. Sub-seismic fractures in foreland fold and thrust belts: insight from the lurestan province, zagros mountains, Iran. Petrol. Geosci. 17, 263–282. https://doi.org/10.1144/1354-079310-043.

Choukroune, P., 1989. The Ecors Pyrenean deep seismic profile reflection data and the overall structure of an orogenic belt. Tectonics 8, 23–39. https://doi.org/10.1029/TC008i001p00023.

Cooper, M., 2007. Structural style and hydrocarbon prospectivity in fold and thrust belts: a global review. Geol. Soc. Spec. Publ. 272, 447–472. https://doi.org/10.1144/GSL.SP.2007.272.01.23.

Cosgrove, J.W., 2015. The association of folds and fractures and the link between folding, fracturing and fluid flow during the evolution of a fold-thrust belt: A brief review. Geol. Soc. Spec. Publ. 421, 41–68. https://doi.org/10.1144/SP421.11.

Crognier, N., Hoareau, G., Aubourg, C., Dubois, M., Lacroix, B., Branellec, M., Callot, J. P., Vennemann, T., 2018. Syn-orogenic fluid flow in the Jaca basin (south Pyrenean fold and thrust belt) from fracture and vein analyses. Basin Res. 30, 187–216. https://doi.org/10.1111/bre.12249.

Cruset, D., Cantarero, I., Benedicto, A., John, C.M., Vergés, J., Albert, R., Gerdes, A., Travé, A., 2020a. From hydroplastic to brittle deformation: controls on fluid flow in fold and thrust belts. Insights from the Lower Pedraforca thrust sheet (SE Pyrenees). Mar. Petrol. Geol. 120, 104517 https://doi.org/10.1016/j.marpetgeo.2020.104517.

Cruset, D., Cantarero, I., Travé, A., Vergés, J., John, C.M., 2016. Crestal graben fluid evolution during growth of the Puig-reig anticline (South Pyrenean fold and thrust belt). J. Geodyn. 101, 30–50. https://doi.org/10.1016/j.jog.2016.05.004.

Cruset, D., Cantarero, I., Vergés, J., John, C.M., Muñoz-López, D., Travé, A., 2018. Changes in fluid regime in syn-orogenic sediments during the growth of the south Pyrenean fold and thrust belt. Global Planet. Change 171, 207–224. https://doi.org/10.1016/j.gloplacha.2017.11.001.

Cruset, D., Vergés, J., Albert, R., Gerdes, A., Benedicto, A., Cantarero, I., Travé, A., 2020b. Quantifying deformation processes in the SE Pyrenees using U–Pb dating of fracture-filling calcites. J Geol Soc London 177, 1186–1196. https://doi.org/10.1144/jgs2020-014.

Delvaux, D., Sperner, B., 2003. new aspects of tectonic stress inversion with reference to the TENSOR program. Geol. Soc. Spec. Publ. 212, 75–100. https://doi.org/10.1144/GSL.SP.2003.212.01.06.

Evans, M.A., Bebout, G.E., Brown, C.H., 2012. Changing fluid conditions during folding: an example from the central Appalachians. Tectonophysics 576–577, 99–115. https://doi.org/10.1016/j.tecto.2012.03.002.

Evans, M.A., Fischer, M.P., 2012. On the distribution of fluids in folds: a review of controlling factors and processes. J. Struct. Geol. 44, 2–24. https://doi.org/10.1016/j.jsg.2012.08.003.

Ferket, H., Swennen, R., Ortuño Arzate, S., Roure, F., 2006. Fluid flow evolution in petroleum reservoirs with a complex diagenetic history: an example from Veracruz, Mexico. J. Geochem. Explor. 89, 108–111. https://doi.org/10.1016/j.gexplo.2005.11.040.

Fischer, M.P., Higuera-Díaz, I.C., Evans, M.A., Perry, E.C., Lefticariu, L., 2009. Fracture-controlled paleohydrology in a map-scale detachment fold: insights from the analysis of fluid inclusions in calcite and quartz veins. J. Struct. Geol. 31, 1490–1510. https://doi.org/10.1016/j.jsg.2009.09.004.

Gallemí Paulet, J., Martínez Ribas, R., Pons, J., 1982. Unidades del Cretácico superior en los alrededores de San Corneli (Provincia de Lleida). J. Iberian Geol. Int. Publ. Earth Sci. 8, 935–948. https://doi.org/10.5209/rev_CGIB.1982.v8.2794.

Garcés, Miguel, López-Blanco, Miguel, Valero, Luis, Beamud, Elisabet, Muñoz, Josep Anton, Oliva-Urcia, Belén, Vinyoles, Andreu, Arbués, Pau, Cabello, Patricia, Cabrera, Lluís, et al., 2020. Paleogeographic and sedimentary evolution of the South Pyrenean foreland basin. Marine Petrol Geol. https://doi.org/10.1016/j.marpetgeo.2019.104105.

García-Senz, J.G., 2002. Cuencas Extensivas del Cretácico. PhD Thesis. University of Barcelona, p. 310.

Garrido-Megías, A., Rios-Aragües, L.-M., Ríos, J.M., 1972. Síntesis geológica del Secundario y Terciario entre los ríos Cinca y Segre. Boletín Geológico y Minero de España 83, 1–47.

Gómez-Garrido, A., 1987. Foraminíferos Planctónicos del Cretácico Superior Surpirenaico. PhD Thesis. Universitat Autònoma de Barcelona, Departament de Geologia.

Grool, A.R., Ford, M., Vergés, J., Huismans, R.S., Christophoul, F., Dielforder, A., 2018. Insights into the crustal-scale dynamics of a doubly vergent orogen from a quantitative analysis of its forelands: a case study of the eastern Pyrenees. Tectonics 37, 450–476. https://doi.org/10.1002/2017TC004731.

Guillaume, Benjamin, Dhont, Damien, Brusset, Stephane, 2008. Three-dimensional geologic imaging and tectonic control on stratigraphic architecture: Upper Cretaceous of the Tremp Basin (south-central Pyrenees, Spain). AAPG Bull. https://doi.org/10.1306/10110706089.

Gutmanis, J., I Oró, L.A., Díez-Canseco, D., Chebbihi, L., Awdal, A., Cook, A., 2018. Fracture analysis of outcrop analogues to support modelling of the subseismic domain in carbonate reservoirs, south-central Pyrenees. Geol. Soc. Spec. Publ. 459, 139–156. https://doi.org/10.1144/SP459.2.

Haines, S.H., 2008. Transformations in Clay-Rich Fault Rocks: Constraining Fault Zone Processes and the Kinematic Evolution of Regions. Ph.D. Thesis, p. 318.

Hurai, V., Huraiová, M., Slobodník, M., Thomas, R., 2015. Stable isotope geochemistry of geofluids. In: Geofluids. Elsevier, pp. 293–344. https://doi.org/10.1016/b978-0-12-803241-1.00009-5.

Kluge, T., John, C.M., Jourdan, A.L., Davis, S., Crawshaw, J., 2015. Laboratory calibration of the calcium carbonate clumped isotope thermometer in the 25-250°C temperature range. Geochem. Cosmochim. Acta 157, 213–227. https://doi.org/10.1016/j.gca.2015.02.028.

Labeur, A., Beaudoin, N.E., Lacombe, O., Emmanuel, L., Petracchini, L., Daëron, M., Klimowicz, S., Callot, J.P., 2021. Burial-deformation history of folded rocks unraveled by fracture analysis, stylolite paleopiezometry and vein cement geochemistry: a case study in the cingoli anticline (umbria-marche, northern apennines). Geosciences (Switzerland) 11, 135. https://doi.org/10.3390/geosciences11030135.

Labraña de Miguel, G., 2004. Evolució de fluids en un anticlinal: estudi pilot en l'anticlinal de Sant Corneli, Pallars Jusà, Lleida. Estudi petrològic i isotopia de carbonats. Master project. Universitat de Barcelona, p. 114.

Lacombe, O., 2012. Do fault slip data inversions actually yield " paleostresses" that can be compared with contemporary stresses? A critical discussion. In: Comptes Rendus - Geoscience. https://doi.org/10.1016/j.crte.2012.01.006.

Lacombe, O., Beaudoin, N.E., Hoareau, G., Labeur, A., Pecheyran, C., Callot, J.-P., 2021. Dating folding beyond folding, from layer-parallel shortening to fold tightening, using mesostructures: lessons from the Apennines, Pyrenees, and Rocky Mountains. Solid Earth 12, 2145–2157. https://doi.org/10.5194/se-12-2145-2021.

Lacroix, B., Buatier, M., Labaume, P., Travé, A., Dubois, M., Charpentier, D., Ventalon, S., Convert-Gaubier, D., 2011. Microtectonic and geochemical characterization of thrusting in a foreland basin: example of the South-Pyrenean orogenic wedge (Spain). J. Struct. Geol. 33, 1359–1377. https://doi.org/10.1016/j.jsg.2011.06.006.

Lanaja, J.M., 1987. Contribucion de la exploracion petrolifera al conocimiento de la geologia de España. IGME 458.

Lefticariu, L., Perry, E.C., Fischer, M.P., Banner, J.L., 2005. Evolution of fluid compartmentalization in a detachment fold complex. Geology 33, 69–72. https://doi.org/10.1130/G20592.1.

Macchiavelli, C., Vergés, J., Schettino, A., Fernàndez, M., Turco, E., Casciello, E., Torne, M., Pierantoni, P.P., Tunini, L., 2017. A new southern north atlantic isochron map: insights into the drift of the iberian plate since the late cretaceous. J. Geophys. Res. Solid Earth 122, 9603–9626. https://doi.org/10.1002/2017JB014769.

Macgregor, D.S., 1996. Factors controlling the destruction or preservation of giant light oilfields. Petrol. Geosci. 2, 197–217. https://doi.org/10.1144/petgeo.2.3.197.

Machel, H.G., Cavell, P.A., 1999. Low-flux, tectonically-induced squeegee fluid flow ("hot flash") into the Rocky Mountain Foreland Basin. Bull. Can. Petrol. Geol. 47 (4), 510–533. https://doi.org/10.35767/gscpgbull.47.4.510.

Martinez Casas, L.F., Travé, A., Cruset, D., Muñoz-López, D., 2019. The Montagut fault system: geometry and fluid flow analysis (southern pyrennes, Spain). In: Petrogenesis and Exploration of the Earth's Interior. Proceedings of the 1st Springer Conference of the Arabian Journal of Geosciences. CAJG-1), Tunisia, pp. 211–214. https://doi.org/10.1007/978-3-030-01575-6_51, 2018.

McArthur, J.M., Howarth, R.J., Shields, G.A., 2012. Strontium isotope stratigraphy. In: The Geologic Time Scale 2012. Elsevier, pp. 127–144. https://doi.org/10.1016/B978-0-444-59425-9.00007-X.

Mencos, J., 2010. Metodologies de reconstrucció i modelització 3D d'estructures geològiques: anticlinal de Sant Corneli-Bóixols (Pirineus centrals). PhD Thesis. Universitat de Barcelona, p. 403.

Mencos, J., Carrera, N., Muñoz, J.A., 2015. Influence of rift basin geometry on the subsequent postrift sedimentation and basin inversion: the Organyà Basin and the Bóixols thrust sheet (south central Pyrenees). Tectonics 34, 1452–1474. https://doi.org/10.1002/2014TC003692.

Mencos, J., Muñoz, J.A., Hardy, S., 2011. Three-dimensional geometry and forward numerical modeling of the sant Corneli anticline (southern Pyrenees, Spain). In: Thrust Fault-Related Folding. American Association of Petroleum Geologists, pp. 283–300. https://doi.org/10.1306/13251342M943434.

Mercedez, R., 2005. Ammonites e Inocerámidos del Santoniense-Campaniense del Bco. de la Podega (Cuenca de Tremp, Pirineos surcentrales): estudio paleontológico y bioestratigráfico. PhD thesis. Univ. Autónoma de Barcelona, Bellaterra.

Mey, P.H.W., Nagtegaal, P.J.C., Roberti, K.J., Hartevelt, J.J.A., 1968. Lithostratigraphic subdivision of post-hercynian deposits in the south-central Pyrenees, Spain. Leidse Geol. Meded. 41, 15–22.

Mitiku, A.B., Bauer, S., 2013. Optimal use of a dome-shaped anticline structure for CO2 storage: a case study in the North German sedimentary basin. Environ. Earth Sci. 70, 3661–3673. https://doi.org/10.1007/s12665-013-2580-z.

Mitra, S., 1990. Fault-propagation folds: geometry, kinematic evolution, and hydrocarbon traps. AAPG (Am. Assoc. Pet. Geol.) Bull. 74, 921–945. https://doi.org/10.1306/0c9b23cb-1710-11d7-8645000102c1865d.

Morley, C.K., 2007. Development of crestal normal faults associated with deepwater fold growth. J. Struct. Geol. 29 (7), 1148–1163. https://doi.org/10.1016/j.jsg.2007.03.016.

Mouthereau, F., Filleaudeau, P.-Y., Vacherat, A., Pik, R., Lacombe, O., Fellin, M.G., Castelltort, S., Christophoul, F., Masini, E., 2014. Placing limits to shortening evolution in the Pyrenees: role of margin architecture and implications for the Iberia/Europe convergence. Tectonics 33, 2283–2314. https://doi.org/10.1002/2014TC003663.

Muñoz, J.A., 2017. Fault-related folds in the southern Pyrenees. AAPG (Am. Assoc. Pet. Geol.) Bull. 101, 579–587. https://doi.org/10.1306/011817DIG17037.

Muñoz, J.A., 1992. Evolution of a continental collision belt: ECORS-Pyrenees crustal balanced cross-section. In: Thrust Tectonics. Springer Netherlands, Dordrecht, pp. 235–246. https://doi.org/10.1007/978-94-011-3066-0_21.

Muñoz-López, D., Alías, G., Cruset, D., Cantarero, I., John, C.M., Travé, A., 2020a. Influence of basement rocks on fluid evolution during multiphase deformation: the example of the Estamariu thrust in the Pyrenean Axial Zone. Solid Earth 11, 2257–2281. https://doi.org/10.5194/se-11-2257-2020.

Muñoz-López, D., Cruset, D., Cantarero, I., Benedicto, A., John, C.M., Travé, A., 2020b. Fluid dynamics in a thrust fault inferred from petrology and geochemistry of calcite veins: an example from the southern Pyrenees. Geofluids 2020, 1–25. https://doi.org/10.1155/2020/8815729.

Nardini, N., Muñoz-López, D., Cruset, D., Cantarero, I., Martín-Martín, J.D., Benedicto, A., Gomez-Rivas, E., John, C.M., Travé, A., 2019. From early contraction to post-folding fluid evolution in the frontal part of the bóixols thrust sheet (Southern Pyrenees) as revealed by the texture and geochemistry of calcite cements. Minerals 9, 117. https://doi.org/10.3390/min9020117.

Oliver, J., 1986. Fluids expelled tectonically from orogenic belts: their role in hydrocarbon migration and other geologic phenomena. Geology 14, 99–102. https://doi.org/10.1130/0091-7613(1986)14<99:FETFOB>2.0.CO;2.

Plaziat, Jean-Claude, 1981. Late cretaceous to late eocene palaeogeographic evolution of southwest Europe. Palaeogeogr. Palaeoclimatol. Palaeoecol. https://doi.org/10.1016/0031-0182(81)90110-3.

Popp, B.N., Podosek, F.A., Brannon, J.C., Anderson, T.F., Pier, J., 1986. 87Sr/86Sr ratios in Permo-Carboniferous sea water from the analyses of well-preserved brachiopod shells. Geochem. Cosmochim. Acta 50, 1321–1328. https://doi.org/10.1016/0016-7037(86)90308-X.

Pujalte, V., Baceta, J.I., Schmitz, B., Orue-Etxebarria, X., Payros, A., Bernaola, G., Apellaniz, E., Caballero, F., Robador, A., Serra-Kiel, J., Tosquella, J., 2009. Redefinition of the ilerdian stage (early Eocene). Geol. Acta 7, 177–194. https://doi.org/10.1344/105.000000268.

Rasbury, E.T., Cole, J.M., 2009. Directly dating geologic events: U-Pb dating of carbonates. Rev. Geophys. 47, RG3001. https://doi.org/10.1029/2007RG000246.

Robert, R., Robion, P., Souloumiac, P., David, C., Saillet, E., 2018. Deformation bands, early markers of tectonic activity in front of a fold-and-thrust belt: example from the Tremp-Graus basin, southern Pyrenees, Spain. J. Struct. Geol. 110, 65–85. https://doi.org/10.1016/j.jsg.2018.02.012.

Roure, F., Andriessen, P., Callot, J.P., Faure, J.L., Ferket, H., Gonzales, E., Guilhaumou, N., Lacombe, O., Malandain, J., Sassi, W., Schneider, F., Swennen, R., Vilasi, N., 2010. The use of palaeo-thermo-barometers and coupled thermal, fluid flow and pore-fluid pressure modelling for hydrocarbon and reservoir prediction in fold and thrust belts. Geol. Soc. Spec. Publ. 348, 87–114. https://doi.org/10.1144/SP348.6.

Roure, F., Choukroune, P., Berastegui, X., Munoz, J.A., Villien, A., Matheron, P., Bareyt, M., Seguret, M., Camara, P., Deramond, J., 1989. Ecors deep seismic data and balanced cross sections: geometric constraints on the evolution of the Pyrenees. Tectonics 8, 41–50. https://doi.org/10.1029/TC008i001p00041.

Roure, F., Swennen, R., Schneider, F., Faure, J.L., Ferket, H., Guilhaumou, N., Osadetz, K., Robion, P., Vandeginste, V., 2005. Incidence and importance of tectonics and natural fluid migration on reservoir evolution in foreland fold-and-thrust belts. Oil Gas Sci. Technol. https://doi.org/10.2516/ogst:2005006.

Séguret, M., Daignières, M., 1986. Crustal scale balanced cross-sections of the Pyrenees; discussion. Tectonophysics 129, 303–318. https://doi.org/10.1016/0040-1951(86)90258-1.

Shackleton, J.R., Cooke, M.L., Vergés, J., Simó, T., 2011. Temporal constraints on fracturing associated with fault-related folding at Sant Corneli anticline, Spanish Pyrenees. J. Struct. Geol. 33, 5–19. https://doi.org/10.1016/j.jsg.2010.11.003.

Sheppard, S.M.F., 1981. Stable isotope geochemistry of fluids. Phys. Chem. Earth 13 (14), 419–445. https://doi.org/10.1016/0079-1946(81)90021-5.

Simó, A., 1986. Carbonate platform depositional sequences, Upper Cretaceous, south-central Pyrenees (Spain). Tectonophysics 129, 205–231. https://doi.org/10.1016/0040-1951(86)90252-0.

Smeraglia, L., Fabbri, O., Choulet, F., Jaggi, M., Bernasconi, S.M., 2022. The role of thrust and strike-slip faults in controlling regional-scale paleofluid circulation in fold-and-thrust belts: insights from the Jura Mountains (eastern France). Tectonophysics 829, 229299. https://doi.org/10.1016/j.tecto.2022.229299.

Srivastava, S.P., Schouten, H., Roest, W.R., Klitgord, K.D., Kovacs, L.C., Verhoef, J., Macnab, R., 1990. Iberian plate kinematics: a jumping plate boundary between Eurasia and Africa. Nature 344, 756–759. https://doi.org/10.1038/344756a0.

Sun, X., Alcalde, J., Gomez-Rivas, E., Struth, L., Johnson, G., Travé, A., 2020. Appraisal of CO2 storage potential in compressional hydrocarbon-bearing basins: global assessment and case study in the Sichuan Basin (China). Geosci. Front. 11, 2309–2321. https://doi.org/10.1016/j.gsf.2020.02.008.

Sun, X., Gomez-Rivas, E., Alcalde, J., Martín-Martín, J.D., Ma, C., Muñoz-López, D., Cruset, D., Cantarero, I., Griera, A., Travé, A., 2021. Fracture distribution in a folded fluvial succession: the Puig-reig anticline (south-eastern Pyrenees). Mar. Petrol. Geol. 132, 105169 https://doi.org/10.1016/j.marpetgeo.2021.105169.

Sun, X., Gomez-Rivas, E., Cruset, D., Alcalde, J., Muñoz-López, D., Cantarero, I., Martín-Martín, J.D., John, C.M., Travé, A., 2022. Origin and distribution of calcite cements in a folded fluvial succession: the Puig-reig anticline (south-eastern Pyrenees). Sedimentology 1–29. https://doi.org/10.1111/sed.12994.

Swennen, R., Muskha, K., Roure, F., 2000. Fluid circulation in the Ionian fold and thrust belt (Albania): implications for hydrocarbon prospectivity. J. Geochem. Explor. 69 (70), 629–634. https://doi.org/10.1016/S0375-6742(00)00043-1.

Tavani, S., Granado, P., Arbués, P., Corradetti, A., Anton Muñoz, J., 2017. Syn-Thrusting, near-surface flexural-slipping and stress deflection along folded sedimentary layers of the Sant Corneli-Bóixols anticline (Pyrenees, Spain). Solid Earth 8, 405–419. https://doi.org/10.5194/se-8-405-2017.

Tavani, S., Mencos, J., Bausà, J., Muñoz, J.A., 2011. The fracture pattern of the Sant Corneli Bóixols oblique inversion anticline (Spanish Pyrenees). J. Struct. Geol. 33, 1662–1680. https://doi.org/10.1016/j.jsg.2011.08.007.

Tavani, S., Snidero, M., Muñoz, J.A., 2014. Uplift-induced Residual Strain Release and Late-Thrusting Extension in the Anaran Mountain Front Anticline, Zagros (Iran). Tectonophysics. https://doi.org/10.1016/j.tecto.2014.08.018.

Tavani, S., Storti, F., Lacombe, O., Corradetti, A., Muñoz, J.A., Mazzoli, S., 2015. A review of deformation pattern templates in foreland basin systems and fold-and-thrust belts: implications for the state of stress in the frontal regions of thrust wedges. Earth Sci. Rev. 141, 82–104. https://doi.org/10.1016/j.earscirev.2014.11.013.

Travé, A., Calvet, F., Sans, M., Vergés, J., Thirlwall, M., 2000. Fluid history related to the Alpine compression at the margin of the south-Pyrenean Foreland basin: the El Guix anticline. Tectonophysics 321, 73–102. https://doi.org/10.1016/S0040-1951(00)00090-1.

Travé, A., Labaume, P., Calvet, F., Soler, A., 1997. Sediment dewatering and pore fluid migration along thrust faults in a foreland basin inferred from isotopic and elemental geochemical analyses (Eocene southern Pyrenees, Spain). Tectonophysics 282, 375–398. https://doi.org/10.1016/S0040-1951(97)00225-4.

Travé, A., Labaume, P., Calvet, F., Soler, A., Tritlla, J., Buatier, M., Potdevin, J.L., Séguret, M., Raynaud, S., Briqueu, L., 1998. Fluid migration during Eocene thrust emplacement in the south Pyrenean foreland basin (Spain): an integrated structural, mineralogical and geochemical approach. Geol. Soc. Spec. Publ. 134, 163–188. https://doi.org/10.1144/GSL.SP.1998.134.01.08.

Travé, A., Labaume, P., Vergés, J., 2007. Fluid systems in foreland fold-and-thrust belts: an overview from the southern Pyrenees. In: Lacombe, O., Roure, F., Lavé, J., Vergés, Jaume (Eds.), Thrust Belts and Foreland Basins, Frontiers in Earth Sciences. Springer Berlin Heidelberg, Berlin, Heidelberg, pp. 93–115. https://doi.org/10.1007/978-3-540-69426-7_5.

Tugend, J., Manatschal, G., Kusznir, N.J., Masini, E., Mohn, G., Thinon, I., 2014. Formation and deformation of hyperextended rift systems: insights from rift domain mapping in the Bay of Biscay-Pyrenees. Tectonics 33, 1239–1276. https://doi.org/10.1002/2014TC003529.

Vandeginste, V., Swennen, R., Allaeys, M., Ellam, R.M., Osadetz, K., Roure, F., 2012. Challenges of structural diagenesis in foreland fold-and-thrust belts: a case study on paleofluid flow in the Canadian Rocky Mountains West of Calgary. Mar. Petrol. Geol. 35, 235–251. https://doi.org/10.1016/j.marpetgeo.2012.02.014.

Veizer, J., 2005. Depositional and diagenetic history of limestones: stable and radiogenic isotopes. In: Isotopic Signatures and Sedimentary Records. Springer-Verlag, Berlin/Heidelberg, pp. 13–48. https://doi.org/10.1007/bfb0009860.

Veizer, J., Ala, D., Azmy, K., Bruckschen, P., Buhl, D., Bruhn, F., Garden, G.A.F., Diener, A., Ebneth, S., Godderis, Y., Jasper, T., Korte, C., Pawellek, F., Podlaha, O.G., Strauss, H., 1999. 87Sr/86Sr, δ13C and δ18O evolution of Phanerozoic seawater. Chem. Geol. 161, 59–88. https://doi.org/10.1016/S0009-2541(99)00081-9.

Vergés, J., 1993. Estudi geològic del vessant sud del Pirineu oriental i central. Evolució cinemàtica en 3D. PhD Thesis. University of Barcelona, pp. 1–199.

Vergés, J., Fernàndez, M., Martínez, A., 2002. The Pyrenean orogen: pre-, syn-, and post-collisional evolution. J. Virtual Explor. 8, 55–74. https://doi.org/10.3809/jvirtex.2002.00058.

Vergés, J., Muñoz, J.A., 1990. Thrust sequences in the southern central Pyrenees. Bull. Soc. Geol. France 6, 265–271. https://doi.org/10.2113/gssgfbull.vi.2.265.

Vilasi, N., Malandain, J., Barrier, L., Callot, J.P., Amrouch, K., Guilhaumou, N., Lacombe, O., Muska, K., Roure, F., Swennen, R., 2009. From outcrop and petrographic studies to basin-scale fluid flow modelling: the use of the Albanian natural laboratory for carbonate reservoir characterisation. Tectonophysics 474, 367–392. https://doi.org/10.1016/j.tecto.2009.01.033.